# Life Cycle Variations of Mesoscale Convective Systems over the Americas

L. A. T. MACHADO

*Aerospace Technical Center/Aeronautical and Space Institute/Atmospheric Science Division, Sao Jose dos Campos, Brazil*

W. B. ROSSOW

*NASA/Goddard Institute for Space Studies, New York, New York*

R. L. GUEDES

*Aerospace Technical Center/Aeronautical and Space Institute/Atmospheric Science Division, Sao Jose dos Campos, Brazil*

A. W. WALKER

*Science Systems and Applications Inc./NASA/GISS, New York, New York*

(Manuscript received 14 February 1997, in final form 9 August 1997)

ABSTRACT

Using *GOES-7* ISCCP-B3 satellite data for 1987–88, the authors studied the evolution of the morphological and radiative properties of clouds over the life cycles of deep convective systems (CS) over the Americas at both tropical and middle latitudes. A deep convective cloud system is identified by adjacent satellite image pixels with infrared brightness temperatures, $T_{IR} < 245$ K (−28°C), that at some time contain embedded convective clusters that are defined by pixel values of $T_{IR} < 218$ K (−55°C). The first part of the analysis computes parameters for each convective system that describe the system areal size, number of convective clusters, fractional convective area, average and maximum size of the convective clusters, shape eccentricity and orientation, mean $T_{IR}$, variance of $T_{IR}$, $T_{IR}$ gradient, and the mean, variance, and gradient of collocated visible reflectances (when available). The second part of the analysis searches a $5° \times 5°$ region centered on each convective system, but in the subsequent image (3-h time separation), to locate possible candidates representing the same system at the later time. For each possible candidate, the method calculates the fraction of areal overlap with the target system and the implied speed and direction of propagation of the whole convective system and the largest convective cluster within the candidate system. The authors review previous studies of the sensitivity of CS statistics to the temperature thresholds used for identification and quantify the effects on these statistics produced by different ways of tracking convective systems. Comparisons of the results from several tracking methods explains how they work and why most of the life cycle statistics are not sensitive to tracking method used. The authors confirm that simple coincidence (as used in most previous studies) works as long as the time step between satellite images is smaller than the time required for significant evolution of the CS: since smaller systems evolve more rapidly, getting accurate results for CS smaller than about 50–100 km probably requires time resolution better than 3 h. The whole dataset has been analyzed by a tropical meteorologist who choses the best candidate at each time step by comparing listings of all the calculated parameters and visually examining each satellite image pair. The whole dataset has also been analyzed by a simple automated procedure. Based on about 3200 cases examined by the meteorologist and about 4700 cases obtained by the completely automated method, the statistical behavior of convective systems over the Americas is described: their mean cloud properties as a function of system size and lifetime, the evolution of their cloud properties over their lifetimes, and their motions. The results demonstrate a direct correspondence between the size and lifetime of mesoscale convective systems and exhibit many common features of their growth, maturation, and decay. Some differences between CS over tropical land and tropical ocean are also apparent.

## 1. Introduction

The structure and evolution of mesoscale clusters of deep convection (hereafter called convective systems, CS) have been studied most extensively in the central United States where there is available an unequaled concentration of surface meteorological instrumentation, particularly rain radars (since e.g., Fujita 1955) and wind profilers, where numerous aircraft experiments have been conducted (since e.g., Plank 1969), and where the longest record of high space and time resolution satellite observations is available (since e.g., Martin and Suomi 1972; Maddox 1980). A large number of studies have revealed the substantial variety and complexity of

*Corresponding author address:* Dr. William B. Rossow, NASA/Goddard Institute for Space Studies, 2880 Broadway, New York, NY 10025.

convective processes and structures in CS (see references and discussion in Cotton and Anthes 1989), but only the assembly of systematic observations from multiple instruments providing multiyear records covering regions of at least 500 km across gives a comprehensive picture of how these systems form, evolve, and decay in this area (e.g., McAnelly and Cotton 1989; Houze et al. 1990). Such a mass of information makes possible detailed theoretical modeling that has identified the essential features of these systems and how they are formed by and interact with their larger-scale environment (e.g., Zhang and Fritsch 1988; Tripoli and Cotton 1989; Moncrieff 1992). However, the variability of mesoscale CS structures and spatial organizations, even in this one area, is strongly related to the larger-scale meteorological forcing (Houze et al. 1990), so comparisons of similar systematic collections of observations of CS under different circumstances would improve understanding of convection and the processes that lead to its organization at mesoscales (Houze 1977; Gamache and Houze 1982, 1983; Mapes and Houze 1992; Machado and Rossow 1993).

Although there have been numerous field experiments (see, e.g., the list in Machado and Rossow 1993), most are limited in space and time and contain only a few occurrences of CS each. Recently, TOGA COARE (Tropical Ocean and Global Atmosphere Coupled Ocean–Atmosphere Response Experiment) obtained an extensive, four-month set of observations of CS over the tropical ocean in the western Pacific (e.g., Chen et al. 1996), which is still being studied. Together with early GATE [GARP (Global Atmospheric Research Program) Atlantic Tropical Experiment] and Marshall Islands datasets, the TOGA COARE observations of CS over tropical oceans are being intensively studied. Less attention has been paid to CS over tropical land (except Velasco and Fritsch 1987; Desbois et al. 1988; Duvel 1989, 1990; Machado and Rossow 1993) and almost none to CS over midlatitude South America in a regime similar to that in the central United States (except Velasco and Fritsch 1987). Planning is under way for an extensive meteorological–hydrological–biological experiment in central Brazil [Large-scale Biosphere–Atmosphere (LBA)] that would provide data similar to TOGA COARE for one of the main concentrations of tropical convection over land. The main purpose of this paper is to present an investigation and survey of the properties and distribution of CS in the Americas, in advance of LBA, to provide comparisons of tropical convection over land with that over oceans and of another midlatitude regime somewhat similar to the central United States that occurs in southern Brazil and northern Argentina (e.g., Guedes and Dias 1984; Velasco and Fritsch 1987).

Although a detailed, long-term survey of CS in the central United States could now be based on observations from an extensive array of Doppler radars and wind and atmospheric profilers, complemented by very high resolution satellite imager and sounder measurements, such an undertaking has not been started. For most of the globe the best statistics can only be obtained from satellite observations. Such a satellite survey would provide the statistics of CS clouds covering the range of meteorological conditions needed to generalize the results of the numerous detailed ground-based and aircraft studies, especially by obtaining a survey that covers the same times and locations. However, satellite observations are not simply a substitute for surface radars and profilers; rather they complement these observations in two important ways. First, most radar observations of convection are made at wavelengths sensitive only to precipitation, although ''cloud'' radars are now coming into use. Most satellite observations of convection, on the other hand, have been made at wavelengths sensitive only to clouds, including those associated with convection, although microwave precipitation determinations are now being made. Second, only the satellite observations can actually cover the very large range of space and timescales involved in CS, including the systems larger than a few hundred kilometers in size, and their interaction with each other and with the planetary-scale atmospheric circulation. A very good illustration of this advantage of satellite observations of CS is provided by the study of multiscale interactions presented by Chen et al. (1996) and Chen and Houze (1997).

Several satellite CS surveys of varying extent have been completed. Most use infrared and/or visible radiance images from geostationary weather satellites (Velasco and Fritsch 1987; Nakazawa 1988; Duvel 1989, 1990; Miller and Fritsch 1991; Machado et al. 1992, 1993; Mapes and Houze 1992, 1993; Laing and Fritsch 1993a, 1993b; Mapes 1993, Machado and Rossow 1993, Chen et al. 1996, Chen and Houze 1997). More recently, microwave radiances measured from polar orbiters have also been examined (McGaughey et al. 1996; McGaughey and Zipser 1996; Mohr and Zipser 1996, but also see Lin and Rossow 1994, 1997). These surveys have raised a number of important questions about deep convection: 1) where do the larger mesoscale systems of convection come from, that is, what explains the observed size distribution (cf. Redelsperger and Clark 1990; Lau et al. 1991; Machado and Rossow 1993); 2) what explains the observed differences in distribution, sizes, properties, and lifetimes of CS over land and oceans (e.g., Velasco and Fritsch 1987; Zipser 1994); 3) what is the significance of the systematic changes of convective cloud-top pressures and anvil cloud optical thicknesses with system size and are they related to the life cycle of these systems (Machado and Rossow 1993); 4) what role do cloud–radiative interactions play in the dynamics of CS (e.g., contrast Chen and Cotton 1988, Lafore and Moncrieff 1989, and Tao et al. 1993); 5) what is the role of CS in the mean radiation balance (Machado and Rossow 1993); 6) how do the larger mesoscale systems interact with the global scale circulation

(e.g., Hartmann et al. 1984; Mapes and Houze 1992; Chen et al. 1996); and 7) are there significant interannual variations of CS (besides in location)? Answers to these questions will come from combining satellite surveys of CS behavior with other comprehensive meteorological and radar datasets, supplemented by the field study datasets, to describe the formation, evolution, and decay of these convective systems.

To help answer these questions the satellite survey methods must be improved in three ways: 1) instead of using ''radiance indices,'' retrieve more physical quantities that are related to cloud and precipitation properties, especially from combinations of different satellite instruments (e.g., visible, infrared, and microwave as in Lin and Rossow 1994, 1997; Liu et al. 1995; Sheu et al. 1996); 2) develop a tracking method to follow the evolution of CS throughout their life cycle; and 3) develop quantitative measures of the internal structure of CS. Many investigators have used very similar methods for identifying a variety of CS in satellite observations (e.g., Maddox 1980; Williams and Houze 1987; Mapes and Houze 1992; Miller and Fritsch 1991; Machado et al. 1992; Mohr and Zipser 1996). Analyses based on these methods have provided comprehensive statistics on the geographic, seasonal, and diurnal frequencies of occurrence and size distributions of CS, especially land–ocean contrasts in these properties. However, use of ''raw'' radiances makes identification of CS somewhat imprecise (as we discuss in the next section) and limits interpretation of the observed variations. If instead of radiances, these methods are applied to the results of analyses that retrieve physical properties of clouds from the satellite radiances, such as the datasets produced by the International Satellite Cloud Climatology Project (ISCCP, Rossow and Schiffer 1991), then the observed changes can be more directly interpreted as changes of the clouds associated with convection (Machado and Rossow 1993). Similarly using microwave retrievals of cloud and precipitation properties would allow for a more physical interpretation. Organizing extensive satellite datasets, such as the ISCCP dataset (now covering more than 14 years) and those that could be produced from microwave measurements (e.g., Liu and Curry 1992, 1993; Lin and Rossow 1994, 1997; McGaughey et al. 1996 and references therein), by identifying individual CS and tracking their evolution has great potential to advance understanding of CS.

Interpretation of some of the first satellite surveys in terms of processes occurring in the CS has been limited by the fact that the statistics were collected for individual observations as independent samples without regard for the stage of development of a particular CS. Such an approach can combine CS of different sizes but at different stages of development (Machado and Rossow 1993). Early composite studies, based on more limited datasets (Frank 1970; Maddox 1983; Houze and Betts 1981; Houze 1982; Cotton et al. 1989; McAnelly and Cotton 1989; Houze et al. 1990), have already shown the variety of significant changes in structure that can occur during the evolution of these systems and the large range of their sizes and durations. Application of a tracking method that determines the age of each system would allow for similar compositing studies using much larger satellite datasets to generalize the results from the detailed field studies.

Martin and Schreiner (1981), Laing and Fritsch (1993a,b), and Rowell and Milford (1993) ''manually'' tracked cloud clusters and squall lines in satellite images. The most extensive such studies have been done by Fritsch and colleagues (Velasco and Fritsch 1987; Miller and Fritsch 1991; Laing and Fritsch 1993a,b), who, together, obtained a total of about 500 cases spread over four geographic regions from a few years of satellite data. These surveys have documented the durations and diurnal phases of the larger CS and illustrate the value of compositing observed properties with life stage. However, such manual tracking (i.e., visual inspection of all images to identify members of single time sequences) is labor intensive and somewhat subjective, so statistics from really large populations are difficult to obtain and difficult to duplicate. Woodley et al. (1980) tracked convective systems for three months in the GATE area with an automated procedure based primarily on a propagation speed criterion. Williams and Houze (1987) proposed another automated method, based on a requirement for the minimum area of superposition between CS in successive images (actually similar to a propagation speed criterion), and applied it to characterize a few cloud clusters in one winter monsoon season near Borneo. Arnaud et al. (1992) proposed a similar automatic method, with some additional criteria to account for the splitting and merging of systems, and applied it to track convective systems over Africa. Their results revealed relationships with surface temperature changes during the life cycle of CS in tropical Africa. Hodges and Thorncroft (1997) have also proposed an analysis method to obtain similar information. Mapes and Houze (1993), Chen et al. (1996), and Chen and Houze (1997) have conducted the most extensive tracking studies to date by applying the Williams and Houze method to satellite infrared images from ISCCP and TOGA COARE covering the tropical western Pacific ocean. The interpretative power of this type of analysis is especially apparent in the analyses of Chen et al. (1996) and Chen and Houze (1997).

Although there is an extensive and growing literature of results based on analyses of satellite observations using similar CS identification and tracking methods (discussed above), the tracking methods have not been systematically tested to understand how they work. Thus, a secondary purpose of this paper is to investigate the sensitivity of our results to the tracking method used by comparing some proposed automated methods with a ''manual'' tracking procedure.

Essentially, a tracking method works by ''recognizing'' a resemblance between two CS in sequential sat-

ellite images, so as part of our investigation of tracking methods, we have developed a number of quantitative descriptions of the structure of CS. Many types of CS have been defined, such as tropical cloud clusters (Frank 1970; Martin and Suomi 1972), squall lines (Houze 1977), non–squall lines (Tollerud and Esbensen 1985), and mesoscale convective complexes (Maddox 1980); but whether these distinctions are all meaningful has not been determined. At this stage, we focus on testing whether these quantitative structure descriptions are useful for tracking CS; but at a later stage, these will become the properties of CS used to describe how these systems behave. Since we use spatially sampled satellite images, we cannot meaningfully determine internal structures in the smaller cloud systems, so we limit our study to CS with radii greater than 100 km.

In section 2 we describe the satellite dataset and the method used to identify CS. In section 3 several structural properties of CS are defined and the different tracking methodologies that are tested are defined. The whole dataset (one year sampled at 3-h intervals) has been analyzed ''manually'' by R. L. Guedes, a tropical meteorologist who is familiar with the appearance in satellite images of convective systems over the Americas. This analysis produced over 3200 cases. The whole dataset has also been analyzed by a simple automated procedure, obtaining over 4700 cases, and parts of the data have been analyzed by several alternative automatic procedures. In section 4 we examine the results from the different tracking methods to understand how they work and to assess the sensitivity of the CS statistics to the tracking method used. Results from the two methods applied to the whole dataset are analyzed in sections 5 and 6 to describe how cloud morphology and radiative properties change during CS life cycles. The last section summarizes our major findings.

## 2. Data and identification method

### *a. ISCCP-B3 data*

The International Satellite Cloud Climatology Project (ISCCP) is an effort to reduce, calibrate, and uniformly format the geostationary and polar-orbiting weather satellite data for climate studies (Schiffer and Rossow 1983). The infrared (IR $\approx$ 11 $\mu$m) and visible (VIS $\approx$ 0.6 $\mu$m) radiance dataset, called ISCCP-B3 data, represents the original satellite images sampled at intervals of 3 h (starting at 0000 UTC each day) and 30 km (actual pixel size is the original infrared resolution, about 7 km for GOES). These data are available since July 1983 (Schiffer and Rossow 1985; Rossow et al. 1996b). The data employed in this study are from GOES-East (subsatellite point at 75°W), which images the Americas, covering the period July 1987–June 1988. An analysis using full resolution GOES-East images was performed for shorter periods to study the effects of the space and time sampling on the results.

The IR and VIS radiances are only weakly influenced by the atmosphere, so that their variations are caused mostly by clouds and the surface (which is why these wavelengths were chosen for these satellites); however, in the Tropics the contribution to the IR signal from the surface is weaker and the signal includes effects of the humidity in the lowest atmosphere. The ISCCP radiance calibrations (Rossow et al. 1996a) are used to convert telemetry counts to VIS scaled radiances (values from 0.0 to 1.0) and IR radiances to brightness temperatures ($T_{IR}$). The VIS scaled radiance, divided by the cosine of the solar zenith angle (also provided in the ISCCP-B3 data), is used as a reflectance (Rf), neglecting the effect of changing Sun–Earth distance. The relative calibration accuracy is estimated to be about $\pm$2% for IR and $\pm$5% for VIS (Brest et al. 1997). The navigation accuracy is estimated to be about 24–30 km (Rossow et al. 1996b).

### *b. Identification of CS*

From the first, infrared images from meteorological satellites have been used to study the behavior of the cloud systems produced by deep convective events (e.g., Houze 1977; Maddox 1980). Since deep convection penetrates into the upper troposphere, the first step in the analysis is to identify all clouds that have tops well above the 450-mb level (midpoint of the troposphere), which corresponds to an altitude of about 6–9 km and temperatures between 245 and 265 K at latitudes equatorward of about 45°. Previous studies have used $T_{IR}$ thresholds in the range between 240 and 255 K to identify high-level clouds associated with convection. Maddox (1980) identified mesoscale convective complexes (MCC) using $T_{IR} < 241$ K. Miller and Fritsch (1991), Mapes and Houze (1993), Laing and Fritsch (1993a,b) and Arnaud et al. (1992) employed similar thresholds. To ensure that the CS we identify might have been produced by deep convection, we use a threshold, $T_{IR} <$ 245 K because a buoyant parcel in the Tropics would have to originate below the 700-mb level to reach this level. This choice is supported by the survey of Fu et al. (1990), who show that there is a break in the frequency of occurrence distribution of all $T_{IR}$ between values of 240 and 255 K. Machado et al. (1992) show that CS with radii less than 73 km rarely contain any cloud tops with $T_{IR} < 231$ K that are associated with active convection (see below). In any case Machado et al. (1992) also show that the shape of the CS size distribution and other attributes of the larger CS are insensitive to the choice of threshold over a range from 240 to 255 K. Both Machado et al. (1992) and Mapes and Houze (1993) have illustrated the near-linear dependence of CS areas or sizes with varying thresholds over a range of 10–20 K that explains the relative insensitivity of distribution statistics to the precise value of the threshold used. Cloud tops with temperatures less than 245 K would have top heights above about 8–9

km; however, use of a radiance threshold means that the thinnest cirrus associated with the CS will be excluded because their apparent temperature is much warmer than their physical temperature, depending on how transparent they are to IR radiation from below. Applying a threshold to the analyzed ISCCP dataset, where physical cloud-top temperatures have been determined, will eliminate this problem in future studies; but for now, to remain consistent with our previous study (Machado and Rossow 1993), we retain the condition that $T_{IR} < 245$ K identifies the high-level clouds of interest.

We define a high-level cloud as a CS only if, at some stage of its existence, it contains active deep convection. Thus, in addition to identification of high-level cloud tops, we must also recognize the presence of active deep convection from the observed cloud-top properties: we use $T_{IR} < 218$ K. Clouds at these temperatures would have tops at heights above 12–13 km. Studies of deep convection based on GATE data (Houze 1977; Leary and Houze 1979; Houze and Betts 1981) and subsequent observations (e.g., Cotton and Anthes 1989) all show that cloud tops over active convection are elevated with respect to the stratiform portion of the CS, which tends to have tops below about 12 km. Many previous studies have followed Maddox (1980) in using $T_{IR} < 221$ K to identify active convective clouds; however, they also require such clouds to be present at all times. Chen et al. (1996) follow Williams and Houze (1987) in using a somewhat lower threshold, $T_{IR} < 208$ K, that identifies cloud areas that correspond closely with radar-detected precipitation; however, they track only these colder-topped objects, excluding the warmer-topped clouds associated with them [however, Mapes and Houze (1993) do examine these warmer-topped clouds]. An identification procedure similar to Maddox's might eliminate both the beginning and ending stages of the CS life cycle, where active convection is not as well developed or absent altogether; however, the CS size limit that we impose in this study may also eliminate the earliest stages. A procedure like Williams and Houze's excludes other (lightly and/or nonprecipitating) clouds that are associated with the larger CS; however, our threshold may exclude the thinnest cirrus. Since we are studying the cloud evolution in these systems, we require only that a CS have detectable convection at some time; we can include more clouds later by applying the detection threshold to physical cloud temperatures, instead of radiances, and can examine earlier/later stages of the system by looking at the images immediately preceding/following the one where the system is first/last detected. Testing these ideas is left to a later study.

Since the same terminology has been used in discussion of several different kinds of observations of convection, there is some confusion. Studies based on ground- and aircraft-based meteorological measurements (temperature, humidity, winds) define a convective cell as a region of high speed updraft within cumulonimbus clouds; the scale of these cells is less than or equal to 20 km (Cotton and Anthes 1989), larger than the typical size of individual satellite fields of view (pixels). Much of the information on the structure of CS comes from surface and aircraft radar studies primarily using low frequency radars that detect only the precipitation-sized particles, not the smaller particles composing the clouds (these systems may also miss some lighter precipitation). The radar cores of these systems, defined by high radar reflectivities caused by heavy rainfall, are larger than the updraft regions because heavy rainfall is associated with both strong updrafts and downdrafts (e.g., Johnson and Houze 1987). In fact, early (e.g., Churchill and Houze 1984) and subsequent studies show that in one system the convective and stratiform rainfall rates vary over the same range but reach their maxima at different times during the life of the system. Nevertheless, it has become conventional to identify the convective cores of these systems by radar reflectivities greater than 20–30 dB*Z* (equivalent to rainfall intensities greater than a few millimeters per hour; see discussion and references in Cotton and Anthes 1989, for example). Cotton and Anthes (1989) show many radar cross sections with ''convective cores'' typically 10–20 km across, but Chong et al. (1987) show a 30-dB*Z* object that is greater than 30 km across, Chauzy et al. (1985) show a ''convective'' region that is 40 km across, Houze and Rappapart (1984) show a ''convective'' feature that is greater than 50 km across, and Houze (1977) shows a 34-dB*Z* object that is about 75 km across. Thus, the radar ''convective'' feature may be several times larger than the dynamic ''convective'' feature (e.g., Houze and Betts 1981).

McAnelly and Cotton (1986) and Chen et al. (1996) both clearly illustrate the structural relations of the ''significant radar features'' with the colder clouds observed by the satellite; the latter show 24-dB*Z* objects greater than 100 km across with smaller embedded features with higher radar reflectivities. They interpret the smaller objects to be the convection, consistent with the smaller scale of the intense updrafts and downdrafts, and the larger objects, which correspond to satellite-observed $T_{IR} < 208$ K, to be the precipitating anvil parts of the system, but this distinction in terms of radar reflectivity (or rainfall rate) is not actually clear cut, since equally light and heavy rainfall rates have been attributed to both the convective and stratiform parts. Although the convective cloud that the satellite sees is likely to be larger than the high-reflectivity features seen in precipitation radars (e.g., Houze and Betts 1981), the size of the individual satellite pixels (about 7 km across for GOES) is small enough that an individual pixel could be identified with these smaller-scale ''convective features.'' Three lines of evidence support use of a threshold between 205 and 220 K to identify such convective clouds. First, as discussed above, is the close correspondence of the heavier precipitation with cloud tops that are this cold, whether they include the immediately adjacent anvil parts of the cumulonimbus or not (e.g.,

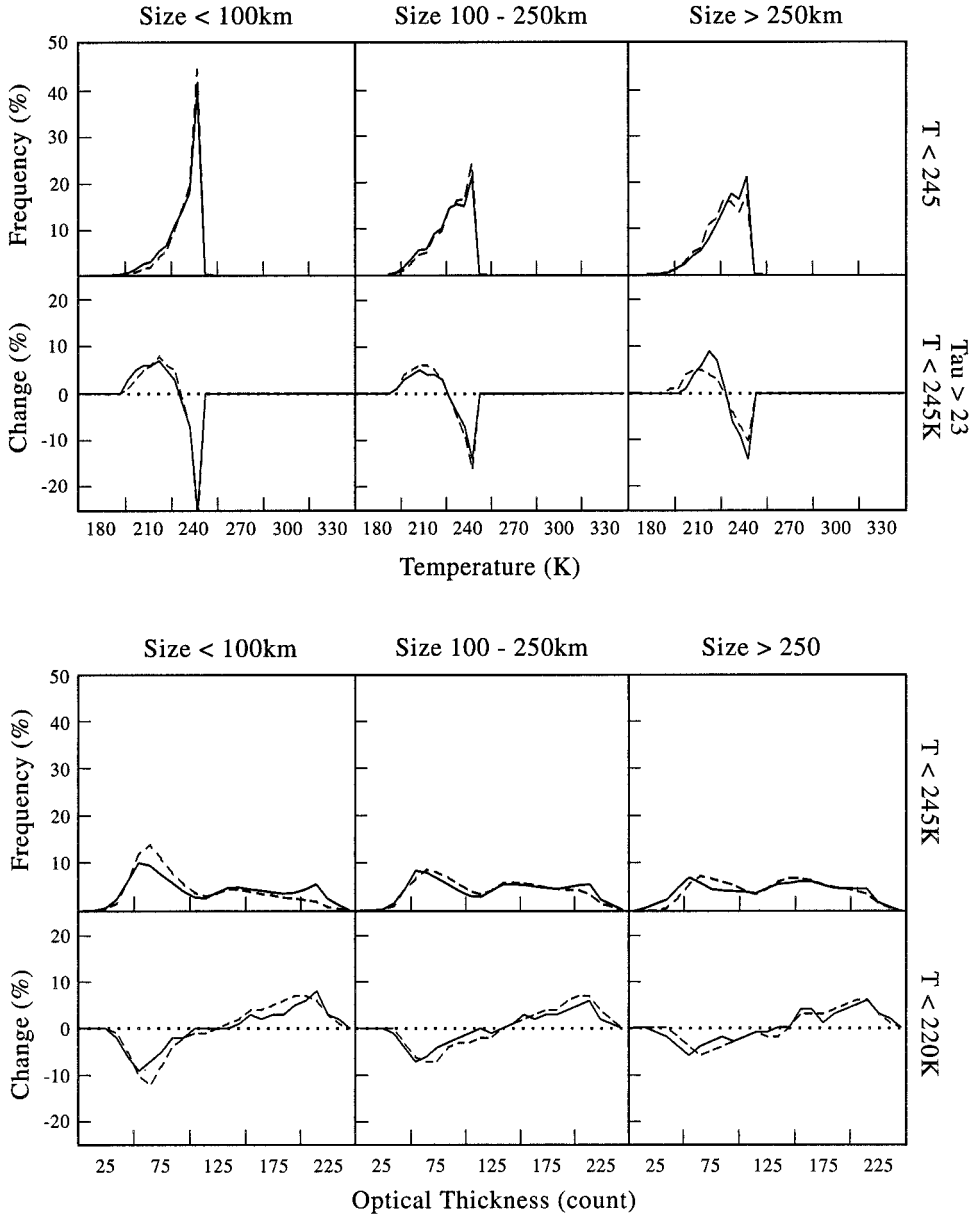


FIG. 1. Top panel: distribution of IR brightness temperatures $T_{IR}$ for all satellite pixels with $T_{IR} < 245$ K. Second panel: relative change in the $T_{IR}$ distribution produced by limiting the population to pixels with $T_{IR} < 245$ and visible optical thickness, $\tau > 23$. Third panel: distribution of $\tau$ for pixels with $T_{IR} < 245$ K. Fourth panel: relative change in the $\tau$ distribution produced by limiting the population to pixels with $T_{IR} < 220$ K (bottom panel). The results are shown for three ranges of the radius of the convective system and separated by whether the system spends the majority of its life over land (solid lines) or water (dashed lines). Data are from *GOES-7* (located at 75°W) for January and July 1990. Visible optical thickness counts represent a nonlinear scale, where a value of 25 corresponds to an optical thickness of 0.75, 75 corresponds to 3.6, 125 corresponds to 9.4, 175 corresponds to 23, and 225 corresponds to 92.

Mohr and Zipser 1996). This close relation allows for relatively accurate statistical estimates of tropical rainfall from satellite infrared measurements (Arkin and Meisner 1987). Second is the high correlation of such cold cloud tops with very high visible optical thicknesses, equivalent to solar reflectivities greater than 0.7 (Fu et al. 1990; Machado et al. 1992), that correspond to large column water amounts in the clouds. These studies also note a nearly linear increase of Rf as $T_{IR}$ decreases below 220 K with little scatter. Figure 1 shows similar results from two months of GOES-EAST ISCCP results. The first and third panels show the distribution of $T_{IR}$ and the cloud visible optical thickness, $\tau$, values for all cloudy pixels with $T_{IR} < 245$ K. The second

panel shows the relative change in the distribution of $T_{IR}$ values produced by limiting the population to pixels that also have an associated $\tau > 23$ (which is equivalent to Rf $> 0.7$). As found before, the larger values of $\tau$ (Rf) are generally concentrated at lower $T_{IR}$ than most other pixels. The fourth panel shows the relative change in the $\tau$ distribution produced by limiting the population to pixels with a lower cutoff value of $T_{IR}$, $< 220$ K. The change shows again that larger values of $\tau$ are found at lower $T_{IR}$. These relationships are generally better for the larger CS (Machado et al. 1992). The third piece of evidence is that collocated visible, infrared, and microwave satellite observations show a strong correspondence of the occurrence of precipitation rates well above a few millimeters per hour with visible optical thicknesses greater than 20–40 (Lin and Rossow 1994, 1997). Thus, we associate satellite pixels with $T_{IR} <$ 218 K with active deep convection because the associated cloud water amounts are large and usually associated with the presence of heavy precipitation. Clusters of such pixels may well contain some stratiform clouds, although these will likely be heavily precipitating as well. Machado et al. (1992) show that the resulting size distributions and statistics are not very different for thresholds of 207 or 218 K, especially for the larger CS.

The next step in the analysis is to transform the satellite images, using the two $T_{IR}$ thresholds (we call $T_{IR}$ = 245 K the CS threshold and $T_{IR}$ = 218 K the CC threshold), into binary images, where values of 0, 1, or 2 are assigned to indicate the absence of any clouds colder than the thresholds, the presence of CS clouds, or the presence of CC clouds, respectively. Then connected ensembles (clusters) of pixels with values equal to 1 or 2 are identified to define a CS–cloud cluster or a CC–cloud cluster by the methodology described by Machado et al. (1992). A cluster of CC clouds is called a convective cluster (hence CC) and is interpreted to represent the convectively active core that contains the convective cells but may also contain some of the closely associated, precipitating anvils. A cluster of CS clouds that contains at least one CC cloud sometime during its life is defined as a convective system and includes all the clouds (precipitating and nonprecipitating) associated with the deep convection (except some of the thinnest cirrus).

For each pixel containing high-level clouds, we assign a cluster identity label and determine the geographical position of the center of mass and the number of pixels in any CS or CC that contains that particular pixel. For each CS and CC, we also calculate the area covered. Since the ISCCP-B3 data are sampled images, we assume that each pixel represents the whole area surrounding it, that is, an area about 30 km across at the subsatellite point. The total area of each CS or CC is then given by the number of pixels in them times 900 km$^2$, the area represented by one pixel. The center of mass is defined by the average latitude and longitude of all pixels belonging to the system. All sizes of CS and CC, even one-pixel clusters, are retained; but in this paper, we focus on CS with radii greater than 100 km.

## 3. Analysis and tracking methods

### *a. Determination of cloud morphological and radiative properties*

All CC locations are compared with the CS locations to identify and count the number of CC embedded within each CS. The size and center of mass position of the largest CC and the average CC size are determined for each CS. These quantities, together with the pixel values of the $T_{IR}$, Rf, latitude, and longitude, are then used to calculate the following parameters.

1) Average $T_{IR}$ and Rf for the CS and for all CC within it:

$$\text{avg rad} = \frac{\sum \text{rad}(i, j)}{N}. \tag{1}$$

The minimum value of $T_{IR}$ and maximum value of Rf in the CS are also recorded.

2) Spatial variances of $T_{IR}$ and Rf for the CS:

$$\text{var rad} = \frac{\left\{\sum \text{rad}^2(i, j) - \left[\sum \text{rad}(i, j)\right]^2\right\}^{1/2}}{N}. \tag{2}$$

3) Average $T_{IR}$ and Rf spatial gradients in the CS:

$$\text{Avg}|\nabla \text{rad}(i, j)| = \frac{1}{N}\left\{\frac{\left[\sum |\text{rad}(k, l) - \text{rad}(i, j)|/d\right]}{M}\right\}. \tag{3}$$

In these expressions, "rad" $= T_{IR}$ or Rf, $N$ is the number of pixels composing the CS, $d$ is the distance in kilometers of pixel $(k, l)$ from the pixel $(i, j)$, and $M$ is the number of pixels at least 0.5° from the pixel $(i, j)$. For CS with the same variances, the average gradient can show if the variability is concentrated in a given region (lower values) or spread over the whole CS area (higher values).

4) Number of CC clusters inside the CS, $N_{CC}$. This number also includes single, isolated CC, represented by a single image pixel, that do not belong to a CC cluster (i.e., a multipixel CC).

5) The effective radii of the CS ($=R_S$) and the largest CC ($=R_C$) and the average radius of all CC inside the CS ($=r_C$). The effective radius is just the radius of a circle with the same area as the cluster area:

$$\text{R} = \left(\frac{\text{area}}{\pi}\right)^{1/2}. \tag{4}$$

We use effective radius (hereafter called radius), in-

stead of cluster area, to give a linear measure of CS size because of the variety of CS shapes observed. Note that, although we assume that the radius of a single pixel CC is 17 km, which may be larger than the actual size, the original image pixel area actually represents a radius of about 4 km, so that it is possible for us to detect the clouds of an isolated convective cloud (although we will overestimate the size of these smaller CC). Note also that other authors report a linear dimension that they define by $(\text{area})^{1/2}$; therefore, our cluster sizes will be smaller than theirs by a factor of $\pi^{1/2} \approx 1.77$. A squall line of adjacent convective cells can be rather small in one dimension, but appear continuous over hundreds of kilometers; such a CC cluster can have relatively large values of $R_C$.

6) Eccentricity of the CS, $\epsilon$. This parameter is defined by the following procedure. First, in image coordinates, we fit a straight line by least squares to the positions of all pixels in the CS; this line becomes the ordinate of new coordinate axes. Second, we project the pixel latitudes ($\text{LAT}_i$) and longitudes ($\text{LON}_i$) onto the new axes ($xx_i$ and $yy_i$):

$$xx_i = \text{LON}_i \cos\beta + \text{LAT}_i \sin\beta \tag{5}$$

$$yy_i = \text{LON}_i \sin\beta + \text{LAT}_i \cos\beta \tag{6}$$

$$\beta = \tan^{-1}\alpha \tag{7}$$

$$\alpha = \frac{\left(N \sum \text{LAT}_i\text{LON}_i - \sum \text{LAT}_i \sum \text{LON}_i\right)}{N \sum \text{LAT}_i^2 - \left(\sum \text{LAT}_i\right)^2}. \tag{8}$$

Then we compute $\epsilon$ as the ratio of the range of abscissa values to the range of ordinate values. If $\epsilon > 1$, the ratio is inverted so that $\epsilon$ is always $\leq 1$. Note that in this definition a circle has $\epsilon = 1$ (not 0):

$$\epsilon = \left|\frac{xx(\max) - xx(\min)}{yy(\max) - yy(\min)}\right|$$

or

$$\epsilon = \left|\frac{yy(\max) - yy(\min)}{xx(\max) - xx(\min)}\right|, \tag{9}$$

whichever is less than 1.

7) The inclination of whichever axis has the largest range of position values is $\beta$ in Eq. (5). When the eccentricity is less than 0.5, this information indicates the orientation of the CS that may be related to the orientation of a cold front. Values of $\epsilon \geq 0.5$ indicate roughly circular shapes for which the axis orientation is not very meaningful.

8) "Convective" fraction (%):

$$\text{Cf} = 100 N_{\text{CC}} \left(\frac{r_C}{R_S}\right)^2. \tag{10}$$

This is just the ratio of the areas covered by clouds with $T_{\text{IR}} < 218$ K and clouds covered by $T_{\text{IR}} < 245$ K. This fraction is not strictly the area covered by convective clouds, since the CC may also include some anvil clouds; but it does represent the relative size of the active (also heavily precipitating) core of the CS.

### b. Tracking methods

The above calculations form the prototype determinations of the internal structure of CS that will be investigated further in a later stage of this work. For now, these quantities are used to try to identify a particular CS in a subsequent image for the purpose of tracking individual CS through their life cycles. We examine several procedures for testing the available information for each CS to determine a match of the same system in a pair of images.

The first step determines the coordinates of a $5° \times 5°$ domain about the center-of-mass location of each CS at time $t_0$ (that has not already been used, see below). The next image at time $t_{0+3\,\text{h}}$ is searched within this domain to locate any CS; all CS at $t_{0+3\,\text{h}}$ within the domain of a particular CS at $t_0$ are possible candidates to be the same CS 3 h later. A single CS at $t_{0+3\,\text{h}}$ may be a candidate match for more than one CS at $t_0$. The size of the initial search area is selected assuming that the propagation velocities of CS are less than or equal to 60 m $\text{s}^{-1}$ (we verify this later). At this stage the direction and speed of propagation for the whole CS and the largest CC within it, together with the fractional area overlap of the whole CS, are calculated for each possible candidate. There are now 28 total parameters for each possible pair of CS (Table 1).

All of the tracking methods determine matches by examining all or a subset of these 28 parameters. In the semiautomatic tracking mode, the computer displays the values of the 28 parameters calculated for a selected CS in the previous image and for all the CS candidates in the subsequent image. Based on the variations of these parameters and a visual inspection of the CS in the images, a meteorologist chooses a matching CS at $t_{0+3\,\text{h}}$. The meteorologist may also decide that there is no match, thus ending that particular sequence. If there is a match, the process is repeated for the next image in sequence until there is no match. This analysis is repeated for each CS that has not been matched with another. In the automatic tracking modes, the differences of each parameter are calculated between a selected CS at $t_0$ and all candidate CS at $t_{0+3\,\text{h}}$. Different procedures are then tested that use different combinations of these parameter differences to determine a match or lack of one. We test some very simple tracking procedures that

TABLE 1. Parameters determined for each convective system, CS; CC refers to the convective clusters within the CS (see text for definitions).

| Parameter | |
|---|---|
| Date and time | (year, month, day, hour) |
| Location of CS center of mass | (latitude, longitude) |
| Radius of CS | (km) |
| Average $T_{IR}$ of CS | (K) |
| Minimum $T_{IR}$ of CS | (K) |
| Variance of $T_{IR}$ of CS | (K) |
| Gradient of $T_{IR}$ of CS | (K km$^{-1}$) |
| Average Rf of CS | |
| Maximum Rf of CS | |
| Variance of Rf of CS | |
| Gradient of Rf of CS | (km$^{-1}$) |
| Eccentricity of CS | |
| Inclination of CS major axis | (degrees from east) |
| Convective fraction | (%) |
| Number of CC | |
| Average radius of CC | (km) |
| Average $T_{IR}$ of CC | (K) |
| Average Rf of CC | |
| Location of largest CC | (latitude, longitude) |
| Radius of largest CC | (km) |
| Propagation speed of CS | (m s$^{-1}$) |
| Propagation direction of CS | (degrees from east) |
| Propagation speed of largest CC | (m s$^{-1}$) |
| Propagation direction of largest CC | (degrees from north) |
| Areal overlap fraction with possible antecedent | (%) |
| Average (weighted) difference of all parameters | (%) |

use a threshold test on only a single quantity to select a match in the subsequent image. The most complex method we test calculates a weighted average of all the differences (the weights have been estimated by comparing the results with other observations) and determines a match by finding the smallest difference (below some maximum). Our investigation strategy is to compare the results of the partly subjective, ''manual'' tracking method (the semiautomatic method), somewhat similar to that used by Laing and Fritch (1993a,b) and earlier investigators, with the objective (automatic) methods, like that used by Williams and Houze (1987). The latter use an area overlap requirement; but, instead of requiring a minimum overlap as a fraction of the CS area regardless of its size, they require a minimum overlap area for CS with radii greater than 80 km that is equivalent to a fractional overlap threshold that decreases with CS size (for smaller CS they employ a constant, but much larger, fractional area overlap threshold)—for the systems that we consider ($R_C > 100$ km), their area overlap threshold is less than or equal to 33%.

To apply these tracking procedures to the ISCCP-B3 images, we need to account for limitations of the time–space resolution: 1) the target and candidate CS radii are restricted to be greater than 100 km (a CS composed of at least 35 image pixels, at least one of which has $T_{IR} < 218$ K at some time during the sequence) to give sufficient statistical weight in the calculations described above and because we expect these larger CS to have longer lifetimes (cf. Velasco and Fritsch 1987); 2) the lifetime of CS is restricted to be at least 6 h, that is, we retain results only for CS identified (tracked) in at least three images, again to ensure significance; 3) we only retain results for sequences that are missing no more than one image during the CS life cycle (a missing image is allowed only if the sequence has four or more images); and 4) we require that a sequence not begin after a missing image or end before a missing image, so that we can be sure that the CS was not present at the preceding and following times.

Another consideration in a tracking analysis is how to deal with splitting or merging systems. In our analysis, we determine only one match and do not ''reuse'' a particular CS in order to ensure that each CS sequence has a unique beginning and end (this is not an inherent feature of our method, however). Hence, if a CS splits, our method will track the system that most closely resembles the original, usually the larger one; the other CS will then be tracked as a separate systems. If a CS merges with a smaller system, we continue to track it, but if a CS merges with a larger system, its life cycle is terminated. As another alternative, Williams and Houze (1987) consider both parts of a split CS to continue to be part of the same system and combine the sequences of two merging CS into a single unique set. Thus, our approach includes all of the same CS in the final statistics as would be included by the Williams and Houze approach, but places the short-lived and smaller CS pieces separately into their size/lifetime categories, whereas the Williams and Houze approach would reduce the average size and lifetime of individual CS somewhat by averaging over all the related pieces. As we will

TABLE 2. Minimum and best match criteria used in tracking methods.

| Parameter | Minimum match criterion | Best match criterion |
|---|---|---|
| Area overlap | >15% | Maximum value |
| Diff. radius | None | Minimum value |
| Diff. min. $T_{IR}$ | None | Minimum value |
| Propagation speed | <60 m $s^{-1}$ | Minimum value |
| Avg. diff. 28-param | <40% (total weighted diff.) | Minimum value |
| Semiautomatic | ''Subjective'' | ''Subjective'' |

show, the number of such split or merge events is relatively small and does not affect the statistics reported here, if only the larger CS are considered; but such events become more important as smaller CS are considered. In future studies of CS structure evolution, such splits and mergers should be monitored to determine whether they are significant events in the life cycle of CS.

Using two, 1-day sets of high-resolution (4 km, 1 h) GOES-East images, we tested the effects of the ISCCP space and time sampling (to intervals of 30 km, 3 h) on the tracking results. The comparison was made using a simple automatic tracking mode that determines a match by the amount of areal overlap between CS in consecutive images. The most noticeable effect of the higher spatial resolution is a significant increase in the total number of CS found, all with sizes much smaller than our cutoff. These smaller-sized systems also generally had much shorter lifetimes, though not always, and would be missed by the 3-h sampling interval used for the ISCCP images. More CC, composed of only one or a few image pixels, were also found at higher resolution. For the larger and longer-lived CS, however, the values of CS and CC radii, eccentricity, minimum, and average $T_{IR}$ all show excellent quantitative agreement. Thus, although the sampling does not affect the results for the larger CS we study, we need to remember, when discussing interpretations of CS behavior, that the smaller systems are not included and that the ISCCP-based results apply only to the upper end of the mesoscale regime.

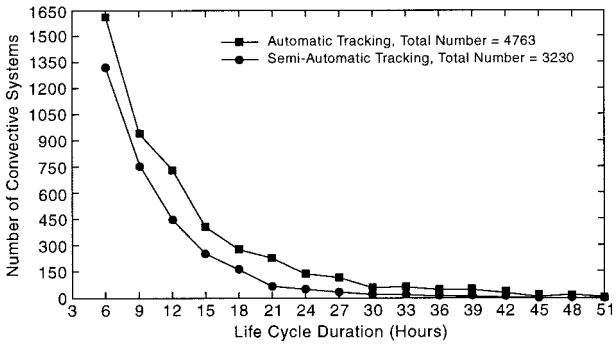


FIG. 2. Number of convective systems obtained from the automatic (''maximum area overlap'' rule) and semiautomatic tracking analyses of one year of GOES-East images as a function of the life cycle duration in hours.

## 4. Comparison of different tracking methods

A tracking method has to make two decisions: 1) if at least one candidate is available in the subsequent image, the procedure must decide whether the match is good enough to continue the time sequence or whether the sequence should be terminated (minimum match criterion); and 2) if more than one candidate is available that meets the minimum criterion, the procedure must decide which single candidate to use to continue a sequence (best match criterion). We comment that the tracking methods used in most previous studies are not completely described in these terms. For example, Laing and Fritsch (1993a,b) do not actually describe their ''tracking'' method, whereas Woodley et al. (1980) do not indicate what is done if two possible candidates are available (although apparently, such a case is labeled as a split) or how it is decided that a system has ''ended.''

We tested six different methods (Table 2). The four simple methods use the value of a single parameter to determine both the minimum and the best match criteria. One method uses the weighted average difference of all 28 parameters in a fully automated analysis and produces similar results to another method that combines an inspection of all the parameters with visual image inspections by a meteorologist in a more subjective analysis. A remarkable result is that most of the CS statistics (see section 5) are not very sensitive to the choice of tracking method, even when the method is not expected to be a particularly good one. In particular, the results from the semiautomatic and the one automatic method (maximum overlap rule) applied to the whole, one-year dataset are nearly the same with one exception: the total number of CS tracked by the automatic method is about 50% larger than that tracked by the meteorologist, with most of the difference occurring in the smaller size (<240 km) and shorter lifetime (≤12 h) categories (see Fig. 2). We found that the propagation trajectories are less noisy and show large-scale circulation features better in the semiautomatic results, suggesting that the visual inspection (subjective) removes (maybe incorrectly) the more ambiguous cases.

The explanation for this insensitivity of the statistics is that, in the majority (≈75%) of cases where there is *any* candidate in the next image, there is only *one* candidate available (regardless of the minimum match criterion). Thus, the only decision to be made in these cases is whether the match is good enough to continue the

time sequence. In only about 20% of the cases with any candidates are there two available, but the second one only exceeds the minimum match criterion about half the time. Consequently, the best match criterion is not actually used very frequently for the larger CS. Note that these statistics also indicate that the number of split events is relatively small, less than or equal to 10% of the cases, if CS smaller than 100 km are ignored. Reexamining these results to identify merge events shows them to be somewhat more numerous, occurring about twice as often for CS with 6-h lifetimes as for CS with lifetimes greater than 21 h, but happening on average for about 20% of the CS. All of these characteristics probably depend on the time interval between images, on the size of the search domain ($\approx$550 km across), and on the fact that we restrict consideration only to the larger CS with radii greater than 100 km. Using shorter time intervals between images and a smaller search domain would reinforce the tendency for ''no choice,'' whereas allowing a larger search domain or smaller CS sizes would create more choices. Stated another way, these results show that the evolution of the larger CS over a period of 3 h is small enough that simple coincidence of location in two satellite images is sufficient for tracking most CS—this assumption is central to almost all previous results employing some form of tracking.

We tested the effects of the size restriction by repeating the analysis of one month of data: in the first case, the size restriction is retained for choosing an initial CS, but smaller CS (radius of at least 41 km) are considered as possible candidate matches. Note that this test is equivalent to testing the effects of changing the temperature threshold used to identify CS; based on the sensitivity study by Mapes and Houze (1993), the change of size used here is approximately equivalent to a 20-K decrease in threshold. In the second case, both the initial and candidate CS can be as small as 41-km radius. Both of these changes significantly increase the number of choices available: in the second case, only about 30% of the cases have only one choice, about 55% have two to four choices, and 15% have more than four choices available (before these fractions were 75%, 25%, and $<$0.1%). However, the number of additional choices that exceed the minimum overlap criterion does not increase; in other words, almost all of the extra possibilities do not generally overlap the CS from the previous image. This result could be a consequence of the 3-h time difference between images allowing sufficient motion of these smaller systems to eliminate overlap (this would only require a propagation speed greater than or equal to 8 m $s^{-1}$); however, the tracking procedure is, in fact, still finding one candidate that does meet the minimum overlap criterion (in this case greater than 15%) because the total number of CS found more than doubles with the smaller size cutoff. Most of these new CS found with a smaller initial size have lifetimes less than or equal to 12 h. These results suggest that splits and mergers become more important if smaller systems are tracked. By restricting our attention to larger systems, the simple tracking methods obtain similar results because there is much less ambiguity. Of the four simple methods tested, the ''maximum area overlap'' rule produces the smallest number of CS and the ''minimum $T_{min}$'' rule produces the largest number of CS. The ''less strict'' methods that produce more total CS also tend to find more small (and rapidly moving) systems and to lengthen average lifetimes, increasing the proportion of CS with lifetimes greater than 24 h. Thus, we conclude that the selection of a tracking method (and cutoff size) affects primarily the total number of CS found and secondarily, the shape of the CS lifetime distribution through the minimum match criterion.

Figure 3 shows the distributions of the parameters, used as criteria in the tracking tests (Table 2), which result when using the ''maximum area overlap'' rule. The shape of these distributions is fairly similar for all the tracking methods (except where noted). Each figure shows the distribution of each parameter for three groups of CS: those chosen as part of a time sequence, those that do not meet the minimum match criterion, and those that meet the minimum match criterion but were rejected in favor of a better-matching CS. The area overlap (Fig. 3a) for chosen CS is significantly larger than the required minimum (15%); the overlap distribution peaks between 50% and 80% [note Williams and Houze (1987) used a 50% criterion for CS smaller than about 80 km and a criterion that decreases linearly with area for larger CS]. Less than 15% of the cases have overlaps below 40%. The rejected candidates have area overlaps overwhelmingly concentrated at 0%. Of course, these results are exaggerated by a selection based on maximizing the overlap; however, even when using the other tracking tests in Table 2, the chosen CS have overlaps greater than 25% and the rejected CS have overlaps concentrated at 0%. In other words, there is a distinct separation of candidate CS that have significant overlap with the CS in the previous image and those that have no overlap. Note that there are also about twice as many candidate CS that overlap as do not, reinforcing the tendency for ''no choice.'' Hence, the use of an ''overlap'' rule naturally separates two distinct groups of candidate CS.

Continuing with the results obtained with the ''maximum overlap'' rule, the chosen candidates also exhibit the smallest size change, generally less than 20%, with a slightly larger fraction of cases where the size is increasing than where the size is decreasing (Fig. 3b). This asymmetry of the distribution is probably affected by our minimum size criterion, which may eliminate the earliest phase of the CS, and our $T_{IR}$ threshold, together with the minimum size criterion, which may eliminate the thin cirrus remnants in the latest phase of the CS (see section 5). The rejected CS are almost always smaller than the CS in the previous image by about 30%–50%. When a ''minimum size difference'' rule is used

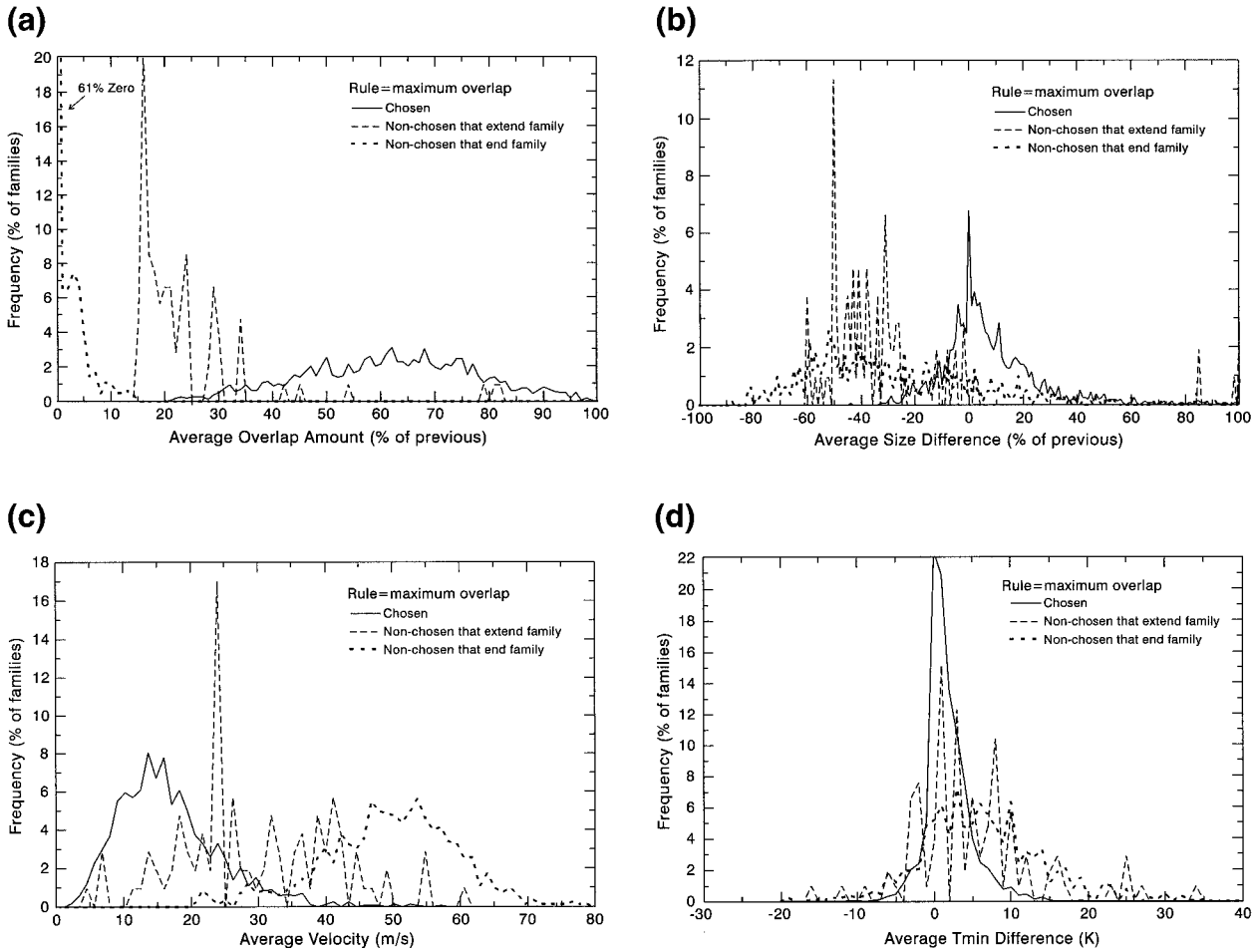


FIG. 3. Distributions of (a) area overlap, (b) radius difference, (c) propagation speed, and (d) difference of the minimum value of $T_{IR}$ obtained by a tracking analysis of one month of GOES-East images using the ''maximum area overlap'' rule. The distributions are for those candidates in the subsequent image that are chosen (1579 families, solid line), that are rejected (825 families, dotted line) because they do not meet the minimum match criterion (overlap at least 15%), and that are rejected because there is a better candidate available (106 families, dashed line).

for tracking, about 30% more CS sequences are obtained that exhibit lower overlap fractions (<30%) and larger propagation speeds (>25 m $s^{-1}$). The CS chosen by the ''maximum overlap'' rule have propagation speeds generally less than 25 m $s^{-1}$ (Fig. 3c), as might be expected, whereas the rejected candidate CS have propagation speeds greater than 30 m $s^{-1}$. When a ''minimum size difference'' rule is used, the chosen CS still have lower propagation speeds than the rejected CS, but the distinction is less clear.

Since area overlap and propagation speed are related, we also examined the statistics obtained using a rule that minimizes the difference in the minimum value of $T_{IR}$ (''minimum $T_{min}$'' rule) to obtain a more independent result. This test is not expected to work very well because there is no reason that the coldest cloud tops should remain constant over the life cycle of these systems (we show that it does not later). This tracking method produces about 50% more CS sequences than the ''maximum overlap'' rule; but the chosen candidates still have distinctly larger area overlap fractions, smaller size differences, and lower propagation speeds than the rejected candidates. Using the ''maximum overlap'' rule, the chosen candidates exhibit distinctly smaller changes in the minimum value of $T_{IR}$ than the rejected candidates (Fig. 3d). The small preference for increasing rather than decreasing $T_{IR}$ shown in the figure may be caused by the size restriction (see section 5). The similarity of results obtained with this scheme arises from the fact that there is really little choice to be made for larger CS when the time step is as short as 3 h.

The statistics that are most sensitive to the choice of tracking method are the total number of CS (that meet minimum size and lifetime criteria), the proportion of CS with lifetimes greater than 24 h, and the average propagation speed. Using ''stricter'' methods that produce fewer CS also reduces the number of long-lived CS and decreases the average propagation speed by 5–

10 m $s^{-1}$. Other results that we present in the next two sections are not sensitive to the particular tracking method employed.

Since we have no independent ''truth'' to verify these results, we cannot tell which method is better. We have made two comparisons with other analyses. The distributions of CS lifetimes obtained by the ''maximum overlap'' rule and the semiautomated method both resemble those obtained by Velasco and Fritsch (1987), but they concentrated on a specific subset of CS, the mesoscale convective complexes, and never describe their tracking method. Thus, this resemblance may only be fortuitous. The CS motion trajectories obtained by our tracking method (see section 5) show very good agreement with those reported in the Tropical Storm Dataset (TSD) available from the National Climatic Data Center (NCDC).

Since the distribution of area overlaps for the ''chosen'' and ''rejected'' CS obtained with all of the tracking methods suggests a separation of the two populations at around 10%–20%, we selected the ''maximum area overlap'' rule (with a 15% threshold) as our primary automated method. We compare the results from the analysis of the whole, one-year dataset based on this automatic tracking method and the semiautomatic tracking method to provide some estimate of the uncertainties.

## 5. Convective system durations and motion trajectories

We have applied both the semiautomatic and automatic (''maximum area overlap'' rule) tracking methods to GOES-East ISCCP-B3 (radiance) images covering July 1987 to June 1988 to study the distribution and life cycle behavior of the larger CS (radii greater than 100 km) over the Americas. Figure 2 shows the number of CS found as a function of lifetime; even with the very strict limit on missing images, we have thousands of cases from one year of data, whereas previous ''manual'' analyses have obtained only a few hundreds of cases from a similar amount of data; with a significant effort, our manual analysis obtained about the same amount of cases. In the semiautomated results, there are about ten times as many CS with 6-h lifetime as there are with 21-h lifetime; in the automatic results, there are about seven times as many 6-h CS as 21-h CS. Velasco and Fritsch (1987) show a much sharper decline in the number of longer-lived CS, by a factor of 10 between lifetimes of about 9 and 18 h; however, they restrict the duration of the CS to the period containing active convection (defined by a temperature threshold of 221 K), whereas we include the inactive stages. In our results, the probability (for all seasons in the Americas) of a CS lifetime less than 9 h is about 60%, of a CS lifetime greater than 24 h is about 5%, and of a CS lifetime greater than 48 h is about 0.5%. The automated results exhibit about double the number of long-lived CS as the manual results. The very low frequency of long-lived systems drives the need to analyze a lot of data to get adequate statistics about the largest CS: for one year, we find only about 200 CS with lifetimes greater than 1 day. In the remainder of this section and the next, we focus on the semiautomatic results because the propagation trajectories are less ''noisy''; however, we will note both sets of results to stress that there is excellent quantitative agreement between the two analyses for all of the remaining statistics discussed.

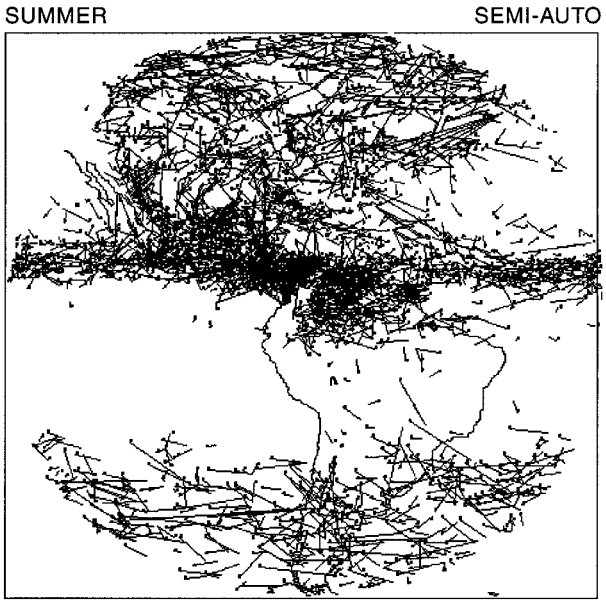


FIG. 4. Trajectories of individual convective systems for boreal summer. The dot at one end of each line identifies the beginning of the trajectory.

Figure 4 illustrates the CS trajectory results by showing the complete dataset for the boreal summer (June 1988, July 1987, and August 1987). At higher latitudes in the winter (southern) hemisphere, the trajectories mainly exhibit the westerly motion of convection associated with cold fronts. In the Tropics the CS propagation in the intertropical convergence zone (ITCZ) is mainly easterly. The trajectories observed during summer and autumn in southern South America are similar to those obtained by Guedes and Dias (1984) and Velasco and Fritsch (1987). The overall average lifetime of the CS is about 10 h, with systems at higher latitudes having slightly longer lifetimes than the tropical systems; Velasco and Fritsch (1987) obtained the same results (overall average lifetime equal to 10 h, with midlatitude MCC lifetimes being about 2 h longer than tropical lifetimes) in their survey of MCC durations over the Americas.

Seasonal charts are constructed showing the mean direction of CS propagation (arrow direction) and the mean CS lifetime (arrow length) for each $5° \times 5°$ region in the GOES-East area (Fig. 5). The mean CS propagation directions resemble the large-scale circulation

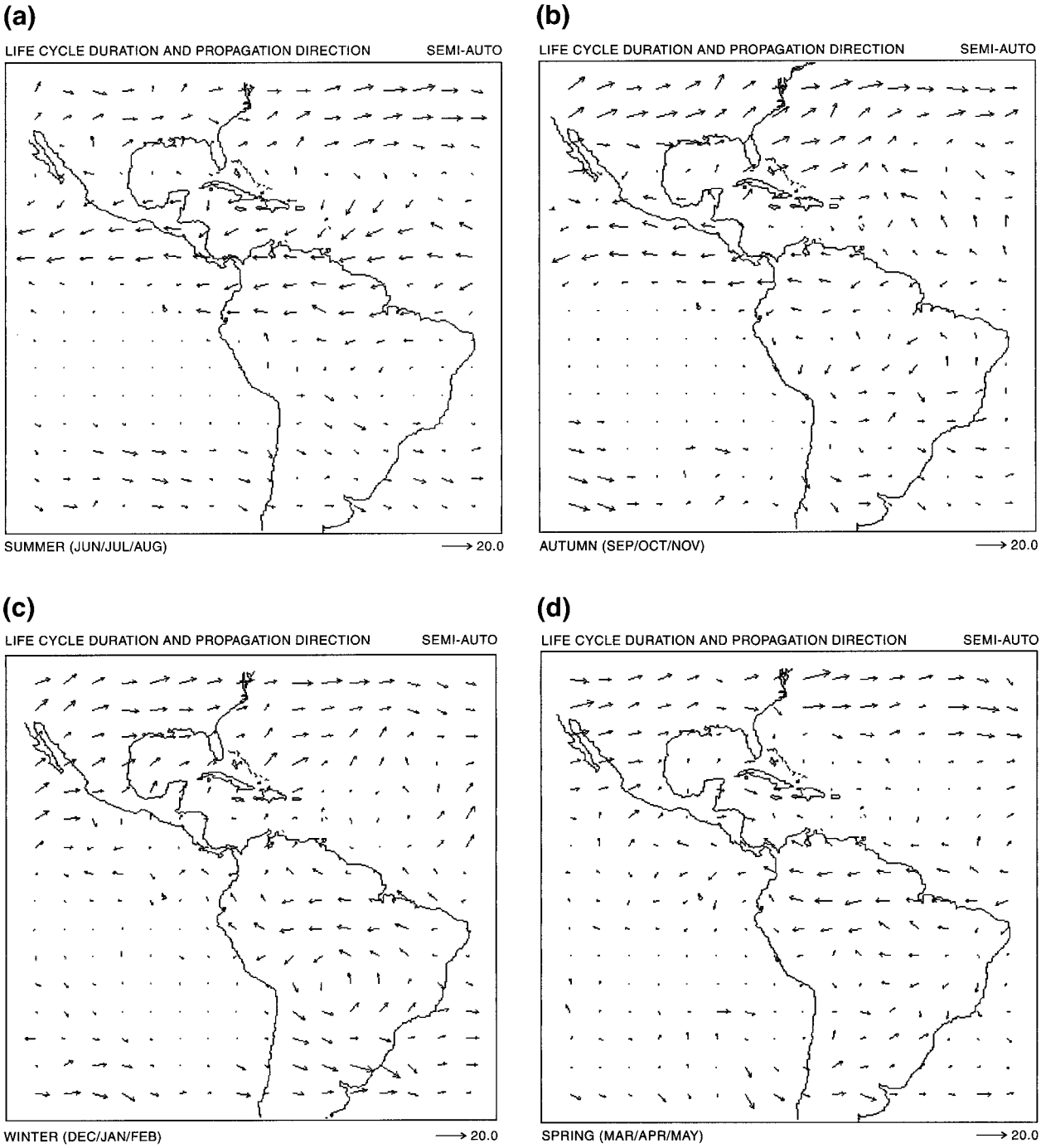


FIG. 5. Average lifetime (in hours, arrow length) and average direction of propagation (arrow direction) of convective systems during boreal (a) summer, (b) autumn, (c) winter, and (d) spring (July 1987–June 1988).

pattern, generally eastward motions at midlatitudes and westward motions near the equator (cf. Lau and Crane 1995). During the boreal summer, the average trajectories in the tropics are all zonally aligned north of the equator and over northern South America, but they become more disorganized (varied directions) during boreal winter with shorter lifetimes. The breakdown of the zonal alignment occurs first in the Carribean sector in boreal autumn. The zonal alignment reforms first over South America in boreal spring, where the CS propagate westward with average lifetimes around 12–18 h. Along the coast of northeast Brazil the CS trajectories reflect the seasonal squall lines formed in land-to-sea breezes as described by Kousky (1980). The CS move generally

eastward over North America in all seasons, but in autumn, the motion is more northeastward and the CS lifetimes are the longest, about 18 h on average. Very few CS occur at any time of year over the subtropical Pacific off South America. During the local summer over the southern Amazon Basin and central South America, the CS trajectories exhibit a southeasterly direction, forming the South Atlantic convergence zone (SACZ), with a mean system lifetime of about 10 h. In local summer, there are many more CS (cf. Velasco and Fritsch 1987) and the mean CS trajectories indicate a prominent anticyclonic circulation pattern (the Bolivia high) that is present mainly during the warm season (Horel et al. 1989). Figures 6a and 6b illustrate the similarity of the CS trajectories obtained by the semiautomatic and automatic tracking methods: all of the features discussed above can be seen in the automatic results, but the mean CS lifetimes are somewhat longer.

Lau and Crane (1995) used motions of large-scale ($\gtrsim$500 km), daily perturbations of cloud optical thicknesses from the ISCCP C1 dataset to build global maps of propagation vectors. Their results show a generally northward displacement of these large-scale perturbations over western South America; however, our results show CS trajectories following the circulation around the Bolivian high. Our trajectories are dominated by the movement of the much more numerous, smaller-sized and shorter-lived CS; but when we isolate the larger-sized and longer-lived CS, we find trajectories similar to those found by Lau and Crane (1995). Thus, we find that the interaction of the CS with the larger-scale circulation differs with CS size. Chen et al. (1996) also find size-dependent interactions of CS in the western Pacific. Combining a more extensive survey of CS covering the whole Tropics for a number of years with analyses of the large-scale circulations might clarify the nature of the size-dependent dynamics of CS.

Figure 7 shows the seasonal variation of the frequency of CS initiations for each $5^\circ \times 5^\circ$ region, defined as the number of times that a CS is first detected there (relative to the total number of CS found in that season). Since we use a lower $T_{IR}$ threshold and limit the minimum radius of CS to at least 100 km, Fig. 7 should be interpreted as the geographical region where mesoscale convective systems begin their mesoscale phase [similar to the results of Maddox (1980) and Velasco and Fritsch (1987)], not where convection begins in general. The CS initiation in all seasons occurs predominantly near the equator and over land, with a tendency to begin on the eastward side of the mountain ranges (cf. Maddox 1980; Velasco and Fritsch 1987; Machado and Rossow 1993), the notable exception being the portion of ITCZ in spring, summer, and autumn over the tropical east Pacific that is mainly associated with strong activity of easterly waves (Riehl 1954). The CS are concentrated closer to the equator in the southern than in the northern hemisphere (cf. Velasco and Fritsch 1987). During boreal summer CS are initiated mainly over northwestern South America and Central America with secondary maxima in North America over Mexico and Florida. In boreal autumn the North American secondary maxima disappear and the initiation region becomes more concentrated just north of the equator in the Pacific. In boreal winter (local summer) the peak initiation region shifts significantly southward into the Amazon Basin with a secondary maximum extending along the Andes in western Argentina, similar to the concentration of CS initiations along the front range of the Rockies in boreal (and local) summer. The boreal spring pattern resembles the autumn pattern, but with more CS initiated along the northeastern coast of Brazil associated with seasonal squall lines as discussed before. Figures 6c and 6d illustrate the similarity of results from the two tracking methods: there are no notable differences in the patterns discussed above.

The distribution of CS initiation frequencies can be used to identify the best locations for planning an experiment in the Amazon region to study CS, such as LBA that will cover a period of at least one year. For LBA, there are three main concentrations of deep convection over tropical land areas: 1) the northeast coast of South America near the outlet of the Amazon River with peak activity from October to May; 2) the northern Brazilian Amazon, Venezuela, and Colombia from June to November; and 3) the southwest Amazon from November to March.

The geographic patterns and seasonal variations of the frequency of CS dissipations, defined as the number of times that a CS is last detected in each region, are similar to the patterns shown in Fig. 7 except that the peak frequencies are shifted westward in the Tropics and eastward at midlatitudes, consistent with the mean propagation trajectories shown in Fig. 5. Thus, most of the CS found over near-coastal oceans originated over land.

## 6. Behavior of CS properties during life cycle

To characterize the average evolution of the CS structure over its life cycle, we sort the CS into groups with the same durations and average all the parameters calculated by the tracking analysis (see section 2) over the whole life cycle and at each 3-h step in the life cycle. Figure 8 shows life-cycle-average properties of the CS for lifetimes from 6 to 27 h: the average system radius, the radius of the largest CC embedded within the CS, the average number of CC contained in the CS, and the minimum value of $T_{IR}$ (called $T_{min}$). Since the average radius of the CS is linearly related to the average lifetime (Fig. 8a), the variation of average CS properties with lifetime can be compared with our previous results (Machado et al. 1992, 1993; Machado and Rossow 1993), which determined the variation of average CS properties with system radius. Systems with a 6-h lifetime have an average radius of 150 km, whereas systems with a 27-h lifetime have a mean radius of 270 km. The au-

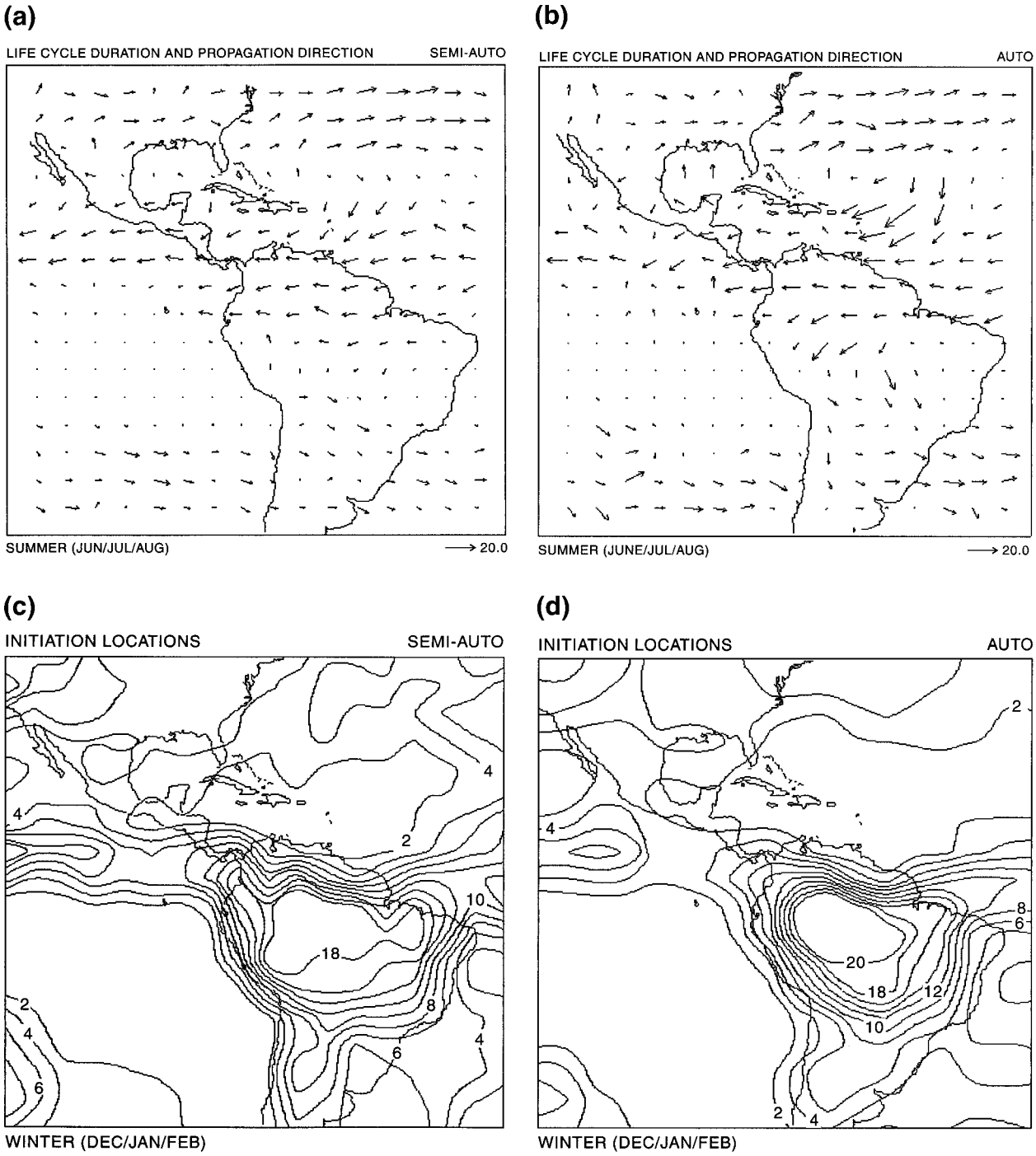


FIG. 6. Comparison of results obtained from the semiautomatic tracking method (left panels) and the automatic tracking method (right panels): (a), (b) mean lifetimes and propagation directions for boreal summer and (c), (d) frequencies of convective system initiation for boreal winter.

tomatic tracking results give somewhat larger radii: 195 km for 6-h lifetimes and 330 km for 27-h lifetimes (henceforth, we will give the corresponding automatic tracking results in parentheses). Figure 8a indicates that average CS radii increase about 6 km for every hour increase in average lifetime. Chen et al. (1996) and Chen and Houze (1997) present the results from their analysis of CS in the tropical western Pacific: these two different figures are drawn very differently and include very different ranges of system lifetimes and sizes, but visual estimates of the slope of a straight line fit to these data suggests an increase of maximum CS size by 13–17 km

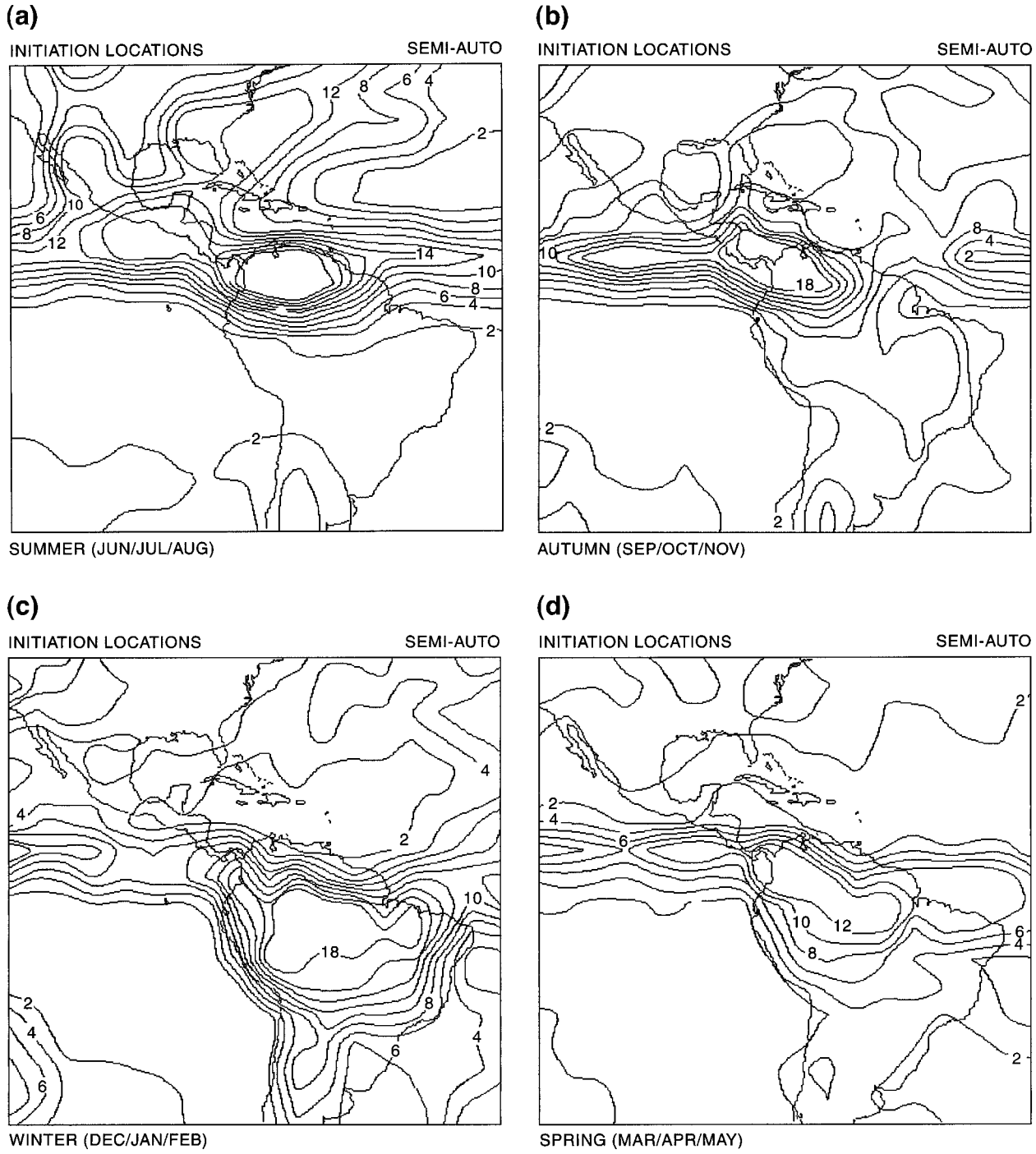


FIG. 7. Frequency of convective system initiations in 5° × 5° regions during boreal (a) summer, (b) autumn, (c) winter, and (d) spring (July 1987–June 1988).

for every hour increase in lifetime. To compare our results with those of Chen et al. (1996), we must account for two differences: 1) Chen et al. use the maximum size of the CS during their lifetimes, whereas we use the average size of the CS over the lifetimes, and 2) Chen et al. define size as the square root of the area, whereas we define size by the radius of a circle with the same area. Reanalyzing our results to obtain the same quantities requires multiplying our slope values by a factor of 1.2 (ratio of maximum to average size) and another factor of $\pi^{1/2} = 1.77$ (radius to square root of area), giving a slope of about 13 km $h^{-1}$. This ex-

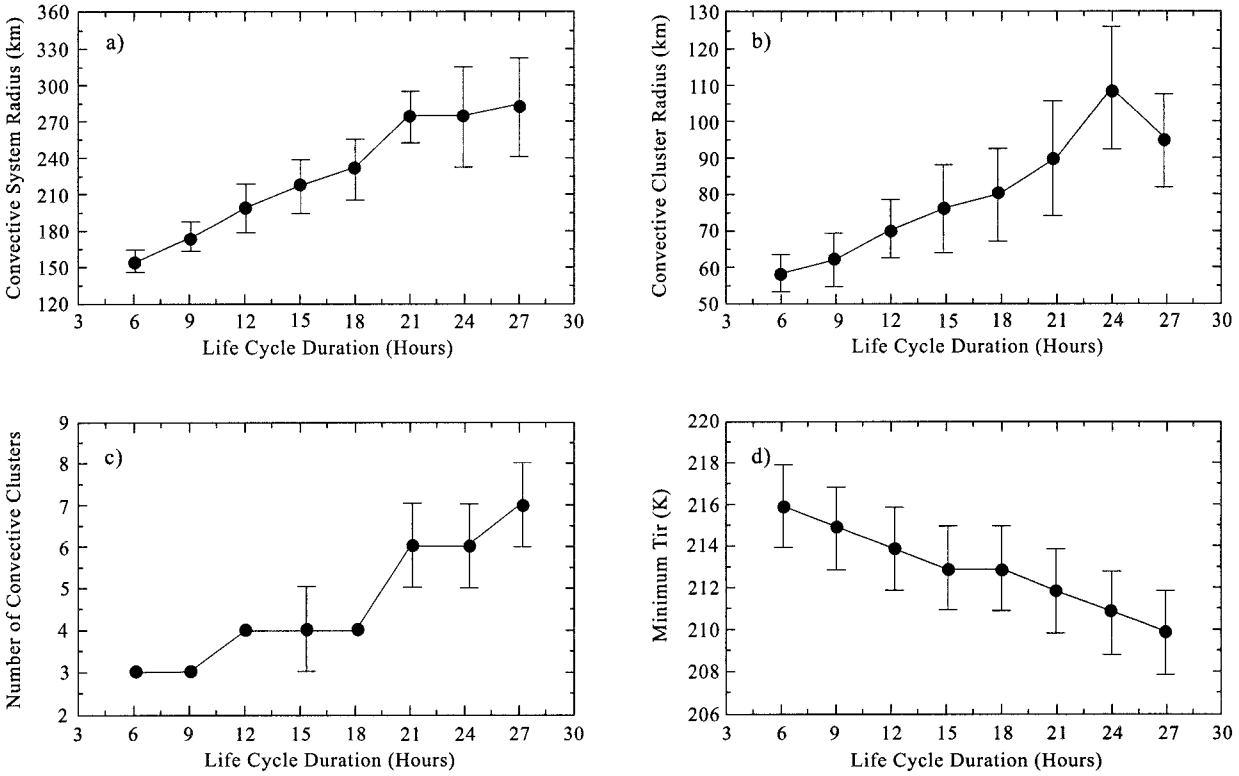


FIG. 8. Average and standard deviation of (a) the effective radius of the convective systems (CS), (b) the effective radius of the largest convective cluster (CC), (c) the number of CC in the CS, and (d) the minimum $T_{IR}$ of the CS as a function of the CS life cycle duration from one year of tracking by the semiautomatic method.

cellent quantitative agreement could mean that the relation of CS size and lifetime is not sensitive to the $T_{IR}$ threshold used, since we use 245 K and Chen et al. use 208 K (actually their objects correspond to our CC), and that there is no significant difference in the size–lifetime relation between predominantly continental and oceanic CS; however, differences caused by different thresholds also might offset the continent–ocean differences. This result requires further study because the longest-lived CS exhibit a tendency to have nearly the same radius, approximately 290 km, which might indicate a change in the dynamics of these systems at this scale.

The explanation for this agreement can be found in the combination of several facts. First, sensitivity studies of CS sizes with temperature threshold have shown that they vary approximately linearly with temperature threshold; however, the shape of the CS size distribution is insensitive to large changes of threshold (cf. Machado et al. 1992; Mapes and Houze 1993). In other words, decreasing the temperature threshold will reduce the average size of a particular CS, but the lifetime of this smaller part is also shorter and its place in the size and lifetime distributions will be taken by the reduction of a still larger system. Second, the same linear size relationship with CS lifetime holds for the largest CC embedded within each CS: the average radius of the largest CC is about 60 (70) km in systems that last 6 h and about 100 (105) km in systems that last 27 h (Fig. 8b). Our CC correspond more closely with the objects studied by Chen et al. (the CC threshold is 218 K versus 208 K), but cannot be directly compared because we do not track the CC, rather we track the CS they are embedded in. Figure 8b implies an increase of average size of about 2 km for each hour of CS (not CC) lifetime increase. The most remarkable difference between our results over tropical land and those of Chen et al. (1996) over tropical ocean is the range of sizes of CC. Chen et al. (1996) find much larger CC (even with a smaller temperature threshold), some as large as 1000 km across, than we find over the Americas, where our largest CC radius is about 140 km (equivalent to sizes of about 250 km in Chen et al.). Third, Machado and Rossow (1993) find that the ratio of CC to CS size is relatively constant at about 0.3 for all CS sizes, giving a rate of increase of CS size with lifetime, estimated from Fig. 8b, of about 13 km $h^{-1}$. Thus, the similarity of our results with those of Chen et al. results from the linear relationships between CC sizes and lifetimes, between CS sizes and lifetimes, and between CC and CS sizes (equivalent to a linear dependence on temperature threshold). Thus, this comparison implies a rough similarity of continental and oceanic CS, but is not suffi-

ciently precise to preclude some smaller systematic differences.

Figures 8c and 8d show that the average number of CC within the CS increases from 3 to 7 (for both tracking methods) and $T_{min}$ decreases from 216 to 210 K (from 214 to 208 K for the automatic tracking) as CS lifetime increases from 6 to 27 h. This result is equivalent to that found by Machado and Rossow (1993) where the average total area of CC's embedded inside the CS [or the probability of finding $T_{IR} < 218$ K (cf. Machado et al. 1992)] increases and the average $T_{min}$ decreases as system radius increases. Machado and Rossow (1993) showed that the second result indicates that the height to which the deep convection penetrates progressively increases as CS size increases. We also find that the average visible reflectance, Rf, increases with increasing system lifetime (not shown), consistent with our previous results. In summary, larger CS tend to have more CC, a larger maximum CC radius, higher CC tops (i.e., lower $T_{min}$), and larger system-average reflectances. The linear variations of average CC number and radius produce a nearly constant average CC fraction (about 30%, no shown) with CS lifetime, consistent with the results of Machado and Rossow (1993); however, as shown below, this fraction varies systematically during the life of the system.

Other parameters are not shown explicitly. The average eccentricity is about 0.6 for all lifetimes, indicating that most CS are quasi-circular [many studies, such as Velasco and Fritsch (1987), have limited their analysis to the nearly circular systems]; however, the eccentricity exhibits more variation among the longer-lived systems, which may indicate that the properties in this category are an average over a mixture of different types of CS. There is a distinct tendency for the distance between the system center of mass and the center of mass of the largest CC to increase as the systems become increasingly eccentric, suggesting that in ''quasi-linear or squall-like'' CS the active convection is located preferentially nearer one side of the system. The spatial variances of $T_{IR}$ and Rf exhibit larger values for the longer-lived CS [note that, since more CS occur at night (Velasco and Fritsch 1987), the Rf statistics are more uncertain]; however the average gradient of $T_{IR}$ is essentially the same for all system durations (but it varies over the life cycle, see below). The average CS propagation speed for all lifetimes is about 12 ($\approx$17) m s$^{-1}$; however, this quantity exhibits very large variations within each lifetime category. The large variability may be caused, in part, by the effect of shape changes on the apparent speed of propagation.

Figure 9 shows the composite life cycle evolution of some CS characteristics, separated into different lifetime categories: CS radius, radius of the largest embedded CC, convective fraction, minimum $T_{IR}$, and $T_{IR}$ gradient. The CS radius evolution has about the same shape over the life cycle for all lifetimes (Fig. 9a). Velasco and Fritsch (1987) have shown separate distributions of CS sizes and durations over the Americas, but do not quantify the relation between sizes (and other cloud properties) and life cycle stage. The CS increase to peak size at about midlife, but the magnitude of the radius increase is usually greater than the decrease. The starting, peak, and final radii are progressively larger as the lifetime increases (these values from the semiautomatic and automatic tracking results are the same to within about 20 km, except that the ending sizes are about 30–50 km larger in the automatic tracking results). The largest CC radius (Fig. 9b) exhibits a similar-shaped distribution; however, the largest CC begins to decrease in size about 3–6 h, before the whole CS does, consistent with many other observations of the evolution of cloud-top temperatures and precipitation (e.g., Johnson and Houze 1987). The time at which the CC is decreasing in area while the CS area is still increasing may be used to forecast the average total lifetime and peak size of CS. The minimum $T_{IR}$ evolution follows that of the largest CC radius (Fig. 9c), reaching its minimum at about the time of peak CC size. McAnelly and Cotton (1989), examining convective systems over the United States, and Arnaud et al. (1992), tracking African convective systems, observed that the decrease of infrared brightness temperature starts before the decrease in total area. The average $T_{IR}$ of the whole CS shows only a small ($\approx$5 K) increase over the life cycle of systems with lifetimes less than or equal to 24 h; longer-lived systems show even less change ($\lesssim$3 K) in average $T_{IR}$. These small changes are produced almost entirely by the variations of the CC cloud-top temperatures; thus, the cloud-top temperatures (heights) of the stratiform clouds outside the CC, which cover a much larger area, vary little (Machado and Rossow 1993). While the average maximum Rf ($Rf_{max}$), indicative of the convective cloud water content, is systematically larger for larger, longer-lived CS, there is little systematic variation of $Rf_{max}$ over the CS life cycle. However, the system average Rf, indicative of the ''anvil'' cloud water content (Machado and Rossow 1993), is generally larger for larger, longer-lived CS and decreases over the CS life cycle except in the first 3–6 h.

The explanation of the life cycle variations of $T_{min}$, average $T_{IR}$, maximum Rf and average Rf is made clear by the variations of the life cycle variations of the convective fraction and the $T_{IR}$ gradient (Figs. 9d and 9e). There is some tendency for the convective fraction to be somewhat larger in the longer-lived CS, but all CS show a general decrease of the convective fraction throughout the lifetime of the system and a corresponding decrease of the gradient of $T_{IR}$. The lower limit on CS radius of 100 km may eliminate the earliest stage of the system's growth where the system size is small, but the convective fraction is even larger than 30% (Machado and Rossow 1993). We interpret these relationships as suggesting that the CS begin at a smaller size, dominated by convective clouds. Higher convective fraction and higher cloud tops (lower $T_{min}$) are correlated

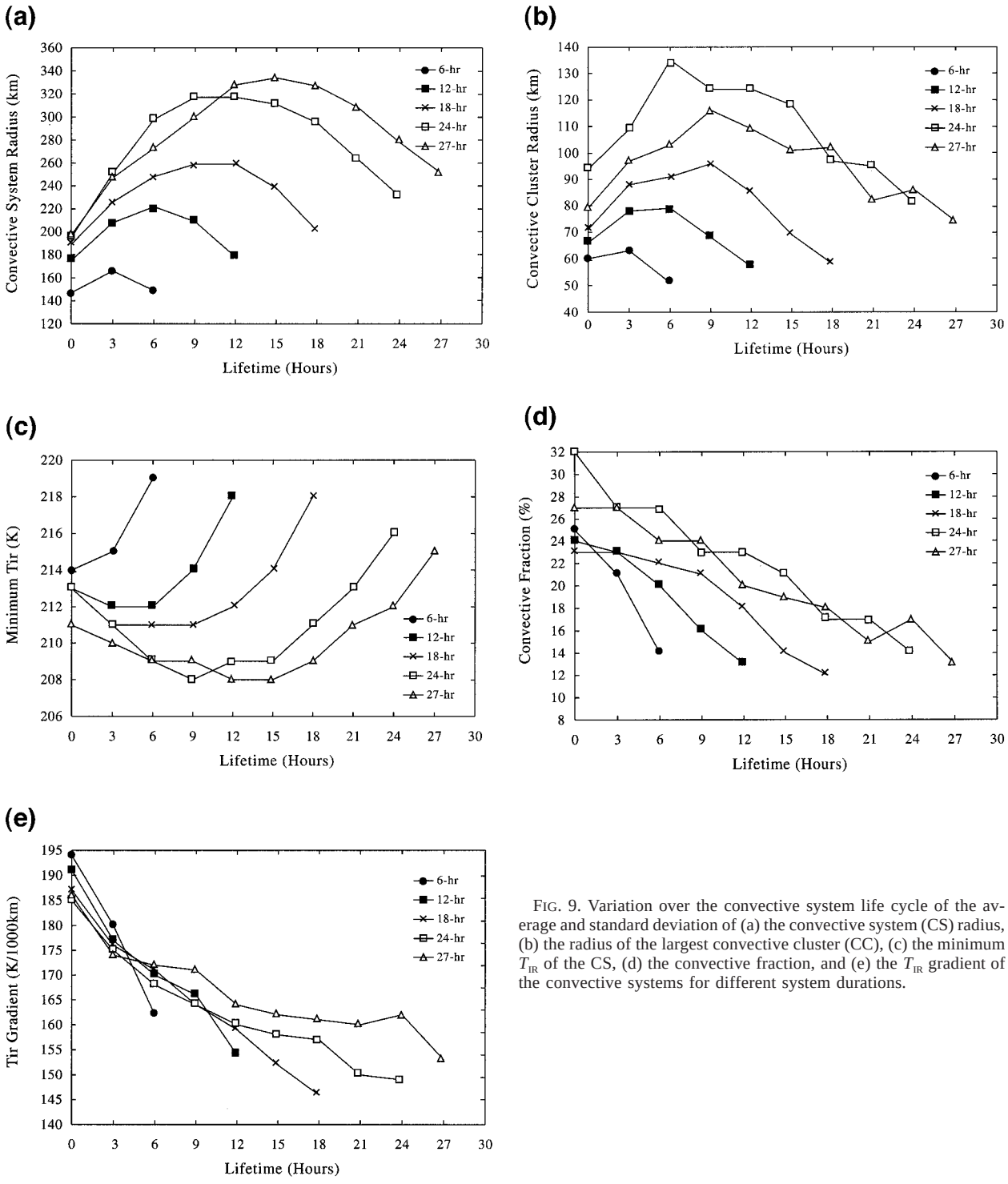


FIG. 9. Variation over the convective system life cycle of the average and standard deviation of (a) the convective system (CS) radius, (b) the radius of the largest convective cluster (CC), (c) the minimum $T_{IR}$ of the CS, (d) the convective fraction, and (e) the $T_{IR}$ gradient of the convective systems for different system durations.

with larger, longer-lived CS with larger average Rf. As the system matures, more anvil cloud is created, reducing the convective fraction. The convective cloud tops reach their peak height and begin to decline, while the anvil cloud area and water content (as indicated by Rf) continue to grow. Finally, as the system begins to decay, the convective fraction and the gradient of $T_{IR}$ decrease even more. The anvil cloud component has nearly constant cloud-top height during the whole life cycle and lasts much longer than the convective component. This discussion of the CS evolution is not new, having been inferred from many previous radar and aircraft studies

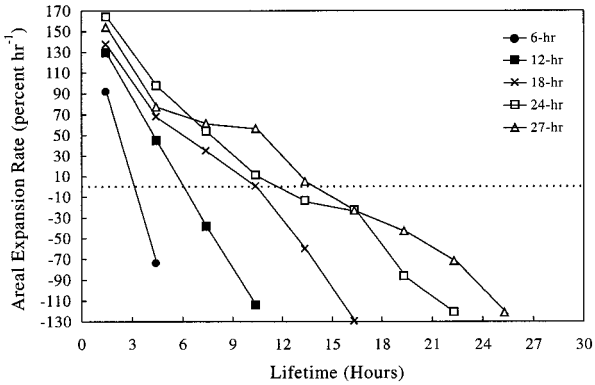


FIG. 10. Variation over the convective system life cycle of the average normalized areal time rate of expansion for different system durations.

(e.g., Leary and Houze 1979; Houze and Betts 1981; Leary and Rappaport 1987; McAnelly and Cotton 1989; Houze et al. 1990); however, our results provide the first systematic and quantitative description of cloud property evolution in these systems and, because of the very large number of cases, indicate the general validity of the previous results. Combining such a detailed analysis of the phasing of the properties of the convective and anvil components of the CS with observations of the meteorology and precipitation, together with diagnoses of radiative and latent heating, can allow examination of cloud-radiative feedbacks on the convective-scale and mesoscale circulations (cf. Fu et al. 1995).

The normalized areal time rate of expansion (AE) is determined from the continuity equation as

$$\mathrm{AE} = \frac{1}{A}\left(\frac{dA}{dt}\right) = \nabla\cdot\mathbf{V}, \tag{11}$$

where $A$ is the cloud area and $\mathbf{V}$ is the horizontal wind vector. The normalized areal time rate of expansion provides, an estimate of the wind divergence at upper levels (Wallace and Hobbs 1977, 400): more rapid areal expansion (contraction) corresponds to larger divergence (convergence). In our case with a 3-h time step, this quantity should be interpreted as the average divergence at the top of the CS. The average variation of AE is calculated for different CS durations and for each time step in the life cycle (Fig. 10). We find that AE is systematically larger at the beginning of the CS life cycle and decreases less rapidly for the larger, longer-lived CS. Tollerud and Esbensen (1985) found a similar evolution of the upper-level wind divergence that lags the boundary layer convergence by 3–6 h. The larger initial growth rates characterizing the larger, longer-lived CS imply larger updraft speeds that are consistent with the higher cloud tops and larger water contents attained in these systems. This result also suggests that the initial value of AE might be used as a predictor of the peak size and duration of CS. The value of AE also provides an indicator of the stage of development (cf. Fig. 9): larger positive values indicating the growth stage, values near 0 indicating the mature stage, and negative values indicating the decay stage.

## 7. Summary and concluding remarks

An automated method for tracking mesoscale convective systems is an important tool for characterizing the behavior of this phenomenon from comprehensive satellite observations. A simple (but more objective) tracking method, based on areal overlap, is shown to work about as well for larger CS as more elaborate methods that look for morphological and radiative similarities of the CS clouds. The semiautomatic method appears to produce less ''noisy'' results for some quantities, but has the disadvantage of being labor intensive and difficult to reproduce. The automatic methods can be applied more easily to much larger datasets, which may offset the somewhat ''noisier'' appearing results. Overall, the small differences in most CS statistics obtained with different tracking methods indicate that most features of the CS life cycle are well determined, even with such simple tracking procedures. This behavior results from the fact that the evolution of the larger CS (radius at least 100 km) over a 3-h time period is small enough that simple coincidence in two sequential images is sufficient for tracking. This principle is central to almost all previous studies using some form of tracking, but our quantitative tests confirm it. However, we also show that a more accurate estimate of the total number of CS (particularly the smaller systems), of the average lifetimes (particularly for the longer-lived systems), and of propagation speeds and directions requires further investigation and testing of tracking methods to understand several subtle issues.

First, the ''beginning'' of a CS time sequence is determined entirely by the CS identification procedure (e.g., temperature threshold and any size criteria), whereas the ''ending'' is determined by the identification procedure and the tracking procedure's minimum match criterion. The size cutoff may also play an important role in ''simplifying'' the choices of candidates to continue a sequence. Because of the spatial sampling and time resolution of the ISCCP dataset, we may not have identified all of the CS at their earliest stage, both because of the size restriction applied and because of the temperature thresholds employed. Moreover, the use of an infrared brightness temperature criterion may miss the thinner cirrus components and reduce the size of some systems below our cutoff, especially at the end of their life cycle. Consequently, the lifetime estimate for individual CS is uncertain by 3–6 h (one or two images). Based on our current methodology, we can investigate possible improvements in this regard by looking next at the behavior of the smaller CS and at the images immediately preceding and following the existing CS sequences to characterize the earliest and latest stages of CS better. We also need to keep track of splitting and

merging events to see whether such systems exhibit any unique structures or properties. If the propagation speeds of some CS can really be larger than about 30–40 m $s^{-1}$, then the overlap criterion in our current tracking procedure is too strict and either needs to be relaxed further or supplemented by other ''similarity'' criteria (e.g., size, $T_{min}$, $Rf_{max}$, CC overlap). Examination of our results in comparison with those from several recent field experiments (e.g., TOGA COARE) will help to improve the accuracy of these aspects of the statistics.

The combination of automated CS identification, clustering, and tracking methods will eventually allow us to survey CS morphological and dynamic characteristics over the globe from a combination of satellite observations, such as the ISCCP-DX cloud properties dataset and microwave cloud and precipitation data. Moreover, these satellite results can be combined with conventional surface and upper-air meteorological observations to examine the interactions of CS with their larger-scale dynamic environment (e.g., Velasco and Fritsch 1987; Goldenberg et al. 1990; Houze et al. 1990; Mapes and Houze 1992). The satellite results could also be combined with Doppler radar surveys to examine precipitation formation processes in more detail. The upcoming Tropical Rainfall Measuring Mission (TRMM) space flight offers an opportunity to combine the analyses of VIS/IR cloud properties, passive microwave cloud and precipitation, and precipitation radar, all observed from a single satellite. A combined satellite analysis allows for an organization of the CS statistics by system size, by duration, and by phase of development, which will give more meaningful insights into the dynamics of these systems. We summarize our first results by focusing on the evolution of the CS properties over their life cycle.

There is a nearly linear relation between the average CS radius (also the maximum radius attained) and its life cycle duration. The same is also true for the average size of the largest convective cluster (close aggregate of multiple convective cells plus associated precipitating anvils) embedded inside the CS. These linear relationships may explain the similarity of results obtained using quite different temperature thresholds to identify CS. These results also show that larger CS tend to have larger CC and last longer: as average CS radius varies from about 150 to 300 km, the largest embedded CC radius varies from about 60 to near 100 km and the system lifetime varies from 6 to 27 h. We note that the study by Chen et al. (1996) of CC in the western tropical Pacific seems to find much larger objects, maximum radii up to approximately 500 km, compared with our maximum radii of about 170 km. Further comparisons are needed to determine if this is a real land–ocean difference in CS.

As CS size and lifetime increase over the ranges mentioned, the average number of convective clusters embedded inside the CS increases from about 3 to about 7 (this includes CC represented by a single satellite pixel) and the average minimum brightness temperature decreases from about 216 to 210 K, suggesting systematically higher tops for the deep convective clouds (cf. Machado and Rossow 1993).

Average convective fraction (ratio of total area of convective clusters to total system area) and brightness temperature gradient are almost constant across all CS lifetime and size categories, but both parameters decrease monotonically during the CS life cycle. These parameters can be used to indicate the development stage of CS independently of their lifetimes. That the convective fraction varies during the mature stage was not determined by Machado and Rossow (1993) because they could not distinguish development stage.

The evolution of CS radius over its life cycle is similar for all categories of system lifetime. The system size increases somewhat more rapidly than it decreases. The size and cloud-top temperature of the largest convective cluster evolve similarly, but the largest CC size begins to decrease and its top temperature begins to increase 3–6 h before the whole CS begins to decrease in size. Thus, the behavior of the coldest cloud temperatures can be used to indicate whether the system is intensifying or dissipating.

Based on previous studies of CS using surface meteorological and radar observations (e.g., Houze 1982; Cotton et al. 1989; McAnelly and Cotton 1989), Machado and Rossow (1993) proposed an interpretation of the systematic variations of CS cloud properties with system size in terms of the life cycle of CS, but could not demonstrate this relationship. The current life cycle results support their proposal, showing that it is possible to follow the ''dynamics'' of CS by the evolution of cloud properties that can be observed from satellites (cf. Houze 1982, 1989; Zipser 1988; Cotton et al. 1989; Mohr and Zipser 1996). By the time the CS reaches a minimum radius of about 100 km, it is still mostly (greater than 30% of the area) composed of a few clusters of very cold cloud tops that contain multiple convective cells and associated precipitating anvil clouds. These clusters quickly reach their maximum extent, cloud-top height, and optical thickness and then decay, while the larger-scale clouds composing the rest of the CS (stratiform component) attain their maximum extent and optical thickness 3–6 h later and then dissipate for a somewhat longer time. For the larger CS that exist for longer than one day, the possible diurnal recurrence of convection and the resulting cloud evolution need to be examined in more detail [we have not examined the diurnal behavior of the CS here; see summaries in Velasco and Fritsch (1987) for the Americas]. To quantify the relationship of the satellite-observed cloud properties and precipitation to the dynamics of CS, we need to develop a much larger dataset, using automatic identification and tracking techniques, so that it can be combined with available aircraft and surface radar and meteorology datasets to provide an adequate statistical sample.

Convective systems with shorter lifetimes and smaller average areas exhibit lower initial areal expansion rates, smaller convective cluster sizes, lower convective cloud tops, and lower anvil cloud reflectances than CS with longer lifetimes and larger average areas. Thus, the initial system (horizontal and vertical) expansion rate and the properties of the convective cluster cloud (vertical and horizontal extent) in the first 3–6 h can be used to estimate CS duration, size, and the water content of the anvil clouds. These relationships also suggest the possibility that the strength of the initial convective updrafts (related to areal expansion rates aloft) determines the maximum height reached by the convective clouds, the amount of water in the large-scale stratiform clouds, and the CS size and duration. Combined with microwave and/or radar observations, these relationships might be extended to include the amount of precipitation produced by CS.

Many of the features of CS evolution, described above, have been noted before for individual cases; however, even this preliminary survey provides quantitative results with a sounder statistical basis (a few thousand cases) that suggests that these features are, in fact, general characteristics of all CS. We have only focused on the similarities of the mesoscale CS; but with such a large number of cases to examine, we can now begin to determine whether the many differences of CS that have been described in previous studies are significant. Notable issues are 1) possible differences of CS behavior when over land and ocean (e.g., Velasco and Fritsch 1987; Machado and Rossow 1993; Mohr and Zipser 1996), particularly whether the apparently larger scale of the organization of CC within CS over the western Pacific as compared with those over the Americas can be confirmed; 2) possible dynamical differences between squall-line and non–squall line systems, other than spatial arrangement of the convection within the system, and between systems that split or merge and systems that do not; 3) possible differences between tropical and higher-latitude systems (Velasco and Fritsch 1987); 4) the interaction of the diurnal variations of convection with the larger CS that last longer than one day (Mapes and Houze 1993; Chen and Houze 1997); 5) whether there are observable differences in the CS that on rare occasions grow into tropical storms or hurricanes/typhoons and whether such a transformation has anything to do with the apparent limit on the sizes of the longer-lived CS; and 6) whether there are noticeable interannual variations in CS characteristics (Velasco and Fritsch 1987).

*Acknowledgments.* Special thanks to José Marcos Silveira for his work on this project. This research was partially supported by Fundação de Amparo à Pesquisa do Estado de São Paulo (FAPESP) Grant 92/4555-9 and by the NASA Global Radiation and Data Analysis program (Dr. Robert A. Schiffer and Dr. Robert J. Curran).

## REFERENCES

Arkin, P. A., and B. N. Meisner, 1987: The relationship between large-scale convective rainfall and cold cloud over the western hemisphere during 1982–1984. *Mon. Wea. Rev.,* **115,** 51–74.

Arnaud, Y., M. Desbois, and J. Maizi, 1992: Automatic tracking and characterization of African convective systems on Meteosat pictures. *J. Appl. Meteor.,* **31,** 443–453.

Brest, C. L., W. B. Rossow, and M. D. Roiter, 1997: Update of radiance calibrations for ISCCP. *J. Atmos. Oceanic Technol.,* **14,** 1091–1109.

Chauzy, S., M. Chong, A. Delannoy, and S. Despiau, 1985: The June 22 tropical squall line observed during COPT 81 experiment: Electrical signature associated with dynamical structure and precipitation. *J. Geophys. Res.,* **90,** 6091–6098.

Chen, S., and W. R. Cotton, 1988: The sensitivity of a simulated extratropical mesoscale convective system to longwave radiation and ice-phase microphysics. *J. Atmos. Sci.,* **45,** 3897–3910.

Chen, S. S., and R. A. Houze, 1997: Diurnal variation and life-cycle of deep convective systems over the tropical Pacific warm pool. *Quart. J. Roy. Meteor. Soc.,* **123,** 357–388.

——, ——, and B. E. Mapes, 1996: Multiscale variability of deep convection in relation to large-scale circulation in TOGA COARE. *J. Atmos. Sci.,* **53,** 1380–1409.

Chong, M., P. Amayenc, G. Scialom, and J. Testud, 1987: A tropical squall line observed during the COPT 81 experiment in West Africa. Part I: Kinematic structure inferred from dual-Doppler radar data. *Mon. Wea. Rev.,* **115,** 670–694.

Churchill, D. D., and R. A. Houze, 1984: Development and structure of winter monsoon cloud clusters on 10 December 1978. *J. Atmos. Sci.,* **41,** 933–960.

Cotton, W. R., and R. A. Anthes, 1989: *Storm and Cloud Dynamics.* Academic Press, 880 pp.

——, M.-S. Lin, R. L. McAnelly, and C. J. Tremback, 1989: A composite model of mesoscale convective complexes. *Mon. Wea. Rev.,* **117,** 765–783.

Desbois, M., T. Kayiranga, B. Gnamien, S. Guessous, and L. Picon, 1988: Characterization of some elements of the Sahelian climate and their interannual variations for July 1983, 1984 and 1985 from the analysis of METEOSAT ISCCP data. *J. Climate,* **1,** 867–904.

Duvel, J.-P., 1989: Convection over tropical Africa and Atlantic Ocean during northern summer. Part I: Interannual and diurnal variations. *Mon. Wea. Rev.,* **117,** 2782–2799.

——, 1990: Convection over tropical Africa and Atlantic Ocean during northern summer. Part II: Modulation by easterly waves. *Mon. Wea. Rev.,* **118,** 1855–1868.

Frank, W. M., 1970: Atlantic tropical systems of 1969. *Mon. Wea. Rev.,* **98,** 307–314.

Fu, Q., S. K. Krueger, and K. N. Liou, 1995: Interactions of radiation and convection in simulated tropical cloud clusters. *J. Atmos. Sci.,* **52,** 1310–1328.

Fu, R., A. D. Del Genio, and W. B. Rossow, 1990: Behavior of deep convective clouds in the tropical Pacific deduced from ISCCP radiances. *J. Climate,* **3,** 1129–1152.

Fujita, T., 1955: Results of detailed synoptic studies of squall lines. *Tellus,* **7,** 405–436.

Gamache, J. F., and R. A. Houze, 1982: Mesoscale air motions associated with a tropical squall line. *Mon. Wea. Rev.,* **110,** 118–135.

——, and ——, 1983: Water budget of a mesoscale convective system in the tropics. *J. Atmos. Sci.,* **40,** 1835–1850.

Goldenberg, S. B., R. A. Houze, and D. D. Churchill, 1990: Convective and stratiform components of a winter monsoon cloud cluster determined from geosynchronous infrared satellite data. *J. Meteor. Soc. Japan,* **68,** 37–63.

Guedes, R. L., and M. A. F. S. Dias, 1984: Case study of severe storms associated with the subtropical jet in South America (in Portuguese). *Proc. of Third Brazilian Meteorological Congress,* Rio de Janeiro, Brazilian Meteorological Society, 289–296.

Hartmann, D. L., H. H. Hendon, and R. A. Houze, 1984: Some implications of the mesoscale circulations in tropical cloud clusters for large-scale dynamics and climate. *J. Atmos. Sci.,* **41,** 113–121.

Hodges, K. I., and C. D. Thorncroft, 1997: Distribution and statistics of African mesoscale convective weather systems based on the ISCCP METEOSAT imagery. *Mon. Wea. Rev.,* **125,** 2821–2837.

Horel, J. D., A. N. Hahmann, and J. E. Geisler, 1989: An investigation of the annual cycle of convective activity over the tropical Americas. *J. Climate,* **2,** 1388–1403.

Houze, R. A., 1977: Structure and dynamics of a tropical squall-line system. *Mon. Wea. Rev.,* **105,** 1540–1567.

——, 1982: Cloud clusters and large-scale vertical motions in the tropics. *J. Meteor. Soc. Japan,* **60,** 396–410.

——, 1989: Observed structure of mesoscale convective systems and implications for large-scale heating. *Quart. J. Roy. Meteor. Soc.,* **115,** 425–461.

——, and A. K. Betts, 1981: Convection in GATE. *Rev. Geophys. Space Phys.,* **19,** 541–576.

——, and E. N. Rappapart, 1984: Air motions and precipitation structure of an early summer squall line over the eastern tropical Atlantic. *J. Atmos. Sci.,* **41,** 553–574.

——, B. F. Smull, and P. Dodge, 1990: Mesoscale organization of springtime rainstorms in Oklahoma. *Mon. Wea. Rev.,* **118,** 613–654.

Johnson, R. H., and R. A. Houze, 1987: Precipitation cloud systems of the Asian monsoon. *Monsoon Meteorology,* C.-P. Cheng and T. N. Krishnamurti, Eds., Oxford University Press, 298–353.

Kousky, V. E., 1980: Diurnal rainfall variation in northeast Brazil. *Mon. Wea. Rev.,* **108,** 488–498.

Lafore, J.-P., and M. W. Moncrieff, 1989: A numerical investigation of the organization and interaction of the convective and stratiform regions of tropical squall lines. *J. Atmos. Sci.,* **46,** 521–544.

Laing, A. G., and M. Fritsch, 1993a: Mesoscale convective complexes in Africa. *Mon. Wea. Rev.,* **121,** 2254–2263.

——, and ——, 1993b: Mesoscale convective complexes over Indian monsoon region. *J. Climate,* **6,** 911–919.

Lau, K. M., T. Nakazawa and C. H. Sui, 1991: Observations of cloud cluster hierarchies over the tropical western Pacific. *J. Geophys. Res.,* **96,** 3197–3208.

Lau, N.-C., and M. W. Crane, 1995: A satellite view of the synoptic-scale organization of cloud properties in midlatitude and tropical circulation systems. *Mon. Wea. Rev.,* **123,** 1984–2006.

Leary, C. A., and R. A. Houze, 1979: The structure and evolution of convection in a tropical cloud cluster. *J. Atmos. Sci.,* **36,** 437–457.

——, and E. N. Rappaport, 1987: The life cycle and internal structure of a mesoscale convective complex. *Mon. Wea. Rev.,* **115,** 1503–1527.

Lin, B., and W. B. Rossow, 1994: Observations of cloud liquid water path over oceans: Optical and microwave remote sensing methods. *J. Geophys. Res.,* **99,** 20 907–20 927.

——, and ——, 1997: Precipitation water path and rainfall estimates for oceans using special sensor microwave images and International Satellite Cloud Climatology Project data. *J. Geophys. Res.,* **102,** 9359–9374.

Liu, G., and J. A. Curry, 1992: Retrieval of precipitation from satellite microwave measurements using both emission and scattering. *J. Geophys. Res.,* **97,** 9959–9974.

——, and ——, 1993: Determination of characteristic features of cloud liquid water from satellite microwave measurements. *J. Geophys. Res.,* **98,** 5069–5092.

——, ——, and R. S. Sheu, 1995: Classification of clouds over the western equatorial Pacific Ocean using combined infrared and microwave satellite data. *J. Geophys. Res.,* **100,** 13 811–13 826.

Machado, L. A. T., and W. B. Rossow, 1993: Structural characteristics and radiative properties of tropical cloud clusters. *Mon. Wea. Rev.,* **121,** 3234–3260.

——, M. Desbois, and J. P. Duvel, 1992: Structural characteristics of deep convective systems over tropical Africa and Atlantic Ocean. *Mon. Wea. Rev.,* **120,** 392–406.

——, J. P. Duvel, and M. Desbois, 1993: Diurnal variations and modulation by easterly waves of the size distribution of convective cloud clusters over West Africa and Atlantic Ocean. *Mon. Wea. Rev.,* **121,** 37–49.

Maddox, R. A., 1980: Mesoscale convective complexes. *Bull. Amer. Meteor. Soc.,* **61,** 1374–1387.

——, 1983: Large-scale meteorological conditions associated with midlatitude, mesoscale convective complexes. *Mon. Wea. Rev.,* **111,** 1475–1493.

Mapes, B. E., 1993: Gregarious tropical convection. *J. Atmos. Sci.,* **50,** 2026–2037.

——, and R. A. Houze Jr., 1992: An integrated view of 1987 Australian monsoon and its mesoscale convective systems. Part I: Horizontal structure. *Quart. J. Roy. Meteor. Soc.,* **118,** 927–963.

——, and ——, 1993: Cloud clusters and superclusters over the oceanic warm pool. *Mon. Wea. Rev.,* **121,** 1398–1415.

Martin, D. W., and V. E. Suomi, 1972: A satellite study of cloud clusters over the tropical North Atlantic Ocean. *Bull. Amer. Meteor. Soc.,* **53,** 135–156.

——, and A. J. Schreiner, 1981: Characteristics of West African and east Atlantic cloud clusters: A survey from GATE. *Mon. Wea. Rev.,* **109,** 1671–1688.

McAnelly, R. L., and W. R. Cotton, 1986: Meso-beta-scale characteristics of an episode of meso-alpha-scale convective complexes. *Mon. Wea. Rev.,* **114,** 1740–1770.

——, and ——, 1989: The precipitation life cycle of mesoscale convective complexes over the central United States. *Mon. Wea. Rev.,* **117,** 784–808.

McGaughey, G., and E. J. Zipser, 1996: Passive microwave observations of the stratiform regions of two tropical oceanic mesoscale convective systems. *J. Appl. Meteor.,* **35,** 1949–1962.

——, ——, R. W. Spencer, and R. E. Hood, 1996: High-resolution passive microwave observations of convective systems over the tropical Pacific Ocean. *J. Appl. Meteor.,* **35,** 1921–1947.

Miller, D,. and J. M. Fritsch, 1991: Mesoscale convective complexes in the western Pacific region. *Mon. Wea. Rev.,* **119,** 2978–2992.

Mohr, K. I., and E. J. Zipser, 1996: Mesoscale convective systems defined by their 85-GHz ice scattering signature: Size and intensity comparison over tropical oceans and continents. *Mon. Wea. Rev.,* **124,** 2417–2437.

Moncrieff, M. W., 1992: Organized convective systems: Archetypal dynamical models, mass and momentum flux theory, and parameterization. *Quart. J. Roy. Meteor. Soc.,* **118,** 819–850.

Nakazawa, T., 1988: Tropical super clusters within intraseasonal variations over the western Pacific. *J. Meteor. Soc. Japan,* **66,** 823–839.

Plank, V., 1969: The size distribution of cumulus clouds in representative Florida populations. *J. Appl. Meteor.,* **8,** 46–67.

Redelsperger, J.-L., and T. L. Clark, 1990: The initiation and horizontal scale selection of convection over gently sloping terrain. *J. Atmos. Sci.,* **47,** 516–541.

Riehl, H., 1954: *Tropical Meteorology.* McGraw-Hill, 392 pp.

Rossow, W. B., and R. A. Schiffer, 1991: ISCCP cloud data products. *Bull. Amer. Meteor. Soc.,* **72,** 2–20.

——, C. L. Brest, and M. Roiter, 1996a: *International Satellite Cloud Climatology Project (ISCCP) New Radiance Calibrations.* WMO/TD-No. 736, World Climate Research Programme (WMO and ICSU), 76 pp.

——, M. D. Roiter, and C. L. Brest, 1996b: *International Satellite Cloud Climatology Project (ISCCP) Updated Description of Reduced Resolution Radiance Data.* WMO/TD-No. 58 (revised), World Climate Research Programme (ICSU and WMO), 163 pp.

Rowell, D. P., and J. R. Milford, 1993: On the generation of African squall lines. *J. Climate,* **6,** 1181–1193.

Schiffer, R. A., and W. B. Rossow, 1983: The International Satellite Cloud Climatology Project (ISCCP): The first project of the World Climate Research Program. *Bull. Amer. Meteor. Soc.,* **64,** 779–784.

——, and ——, 1985: ISCCP global radiance data set: A new resource for climate research. *Bull. Amer. Meteor. Soc.*, **66,** 1498–1505.

Sheu, R.-S., J. A. Curry, and G. Liu, 1996: Satellite retrieval of tropical precipitation using combined International Satellite Cloud Climatology Project DX and SSM/I data. *J. Geophys. Res.*, **101,** 21 291–21 301.

Tao, W.-K., J. Simpson, C.-H. Sui, B. Ferrier, S. Lang, J. Scala, M.-D. Chou, and K. Pickering, 1993: Heating, moisture, and water budgets of tropical and midlatitude squall lines: Comparisons and sensitivity to longwave radiation. *J. Atmos. Sci.*, **50,** 673–690.

Tollerud, E. I., and S. K. Esbensen, 1985: A composite life cycle of nonsquall mesoscale convective systems over the tropical ocean. Part I: Kinematic fields. *J. Atmos. Sci.*, **42,** 823–837.

Tripoli, G. J., and W. R. Cotton, 1989: Numerical study of an observed orogenic mesoscale convective system. Part 2: Analysis of governing dynamics. *Mon. Wea. Rev.*, **117,** 305–328.

Velasco, I., and J. M. Fritsch, 1987: Mesoscale convective complexes in the Americas. *J. Geophys. Res.*, **92,** 9591–9613.

Wallace M. J., and P. V. Hobbs, 1977: *Atmospheric Science: An Introduction Survey*. Academic Press, 467 pp.

Williams M., and R. A. Houze, 1987: Satellite-observed characteristics of winter monsoon cloud clusters. *Mon. Wea. Rev.*, **115,** 505–519.

Woodley, W. L., C. G. Griffith, J. S. Griffin, and S. C. Stromatt, 1980: The inference of GATE convective rainfall from SMS-1 imagery. *J. Appl. Meteor.*, **19,** 388–408.

Zhang, D.-L., and J. M. Fritsch, 1988: Numerical sensitivity experiments of varying model physics on the structure, evolution and dynamics of two mesoscale convective systems. *J. Atmos. Sci.*, **45,** 261–293.

Zipser, E. J., 1988: The evolution of mesoscale convective systems: Evidence from radar and satellite observations. *Tropical Rainfall Measurements*, J. S. Theon and N. Fugono, Eds., Deepak, 159–166.

——, 1994: Deep cumulonimbus cloud systems in the tropics with and without lightning. *Mon. Wea. Rev.*, **122,** 1837–1851.